CANCER

Coordinate tumor-antigen uptake and dendritic cell activation by chimeric antigen receptors

Yahya Mohammadzadeh[1,2,3], Vojislav Gligorovski[4,5], Olga Egorova[1,3], Gabriele Casagrande Raffi[1,2,3], Jort J. van der Schans[1,2,3], Ali Ghasemi[1,2,3], Katharina Jonas[1,2,3,6], Bruno Torchia[1,2,3], Alan Guichard[1,2,3], Rachel Marcone[2,7], Amaia Martinez-Usatorre[1,2,3]†, Anna Köck[3,8,9], Raphael Genolet[8,9], Nadine Fournier[2,7], Tatiana V. Petrova[3,8,9], Daniel E. Speiser[3,8], Sahand Jamal Rahi[4], Nahal Mansouri[1,2,3,5], Michele De Palma[1,2,3]*

Effective antitumor immunity requires dendritic cells (DCs) to internalize, process, and present tumor antigens to T cells. Adoptive transfer of DCs that were loaded ex vivo with tumor antigens has been shown to stimulate antitumor immunity in patients with cancer, but clinical responses have been mixed. To address the limitations of traditional DC-based therapies, we constructed and functionally screened a panel of chimeric antigen receptors (CARs) optimized for expression and activity in DCs. Through this screening, we identified key functional components that guided the development of an inducible platform centered on an instructive chimeric antigen receptor (iCAR). This iCAR enabled DCs to (i) recognize a surface molecule present on cancer cells or their extracellular vesicles (EVs), such as disialoganglioside GD2 (expressed in melanoma and other tumors of neuroectodermal origin) or HER2 (expressed in some epithelial cancers), thereby promoting the acquisition of tumor-derived material containing putative tumor antigens; (ii) undergo immunostimulatory activation to prime antigen-specific T cells via both cross-dressing and cross-presentation; and (iii) transactivate the expression of the therapeutic cytokine interleukin-12 (IL-12) in response to antigen uptake. The iCAR converted melanoma-derived EVs from immunosuppressive to stimulatory cues for DCs in cell culture assays. Moreover, systemic administration of iCAR-DCs enhanced antigen-specific T cells, expanded low-frequency T cell clonotypes, and delayed tumor growth in immunotherapy-resistant melanoma models without the need for ex vivo antigen loading or cell maturation. iCAR-DCs may therefore provide a platform for antigen-agnostic cancer immunotherapy that integrates antigen uptake with programmable DC activation.

INTRODUCTION

Directing or enabling the immune system to recognize and eliminate cancer cells has become a clinically validated approach for treating cancer. In addition to clinically approved immune checkpoint blockade targeting the programmed death-1 (PD-1) and cytotoxic T lymphocyte–associated protein 4 pathways (*1*, *2*), cell therapies based on genetically modified T cells have shown notable clinical efficacy in some hematological cancers as well as promising activity in selected solid tumor types (*3*–*5*). Dendritic cells (DCs) have also received considerable attention because of their ability to present tumor-associated antigens and neoantigens (together termed TAAs hereafter) and orchestrate immune responses against cancer. Personalized treatments based on patient-derived DCs pulsed with TAAs ex vivo have been extensively explored, demonstrating safety and proof of immunogenicity in multiple clinical trials (*6*–*10*). However, the suboptimal antigen presentation and migratory capacities of the manufactured cell product may have limited their clinical efficacy in most trials (*8*). Efforts to bolster the efficacy of DC-based therapies have recently focused on identifying DC subsets with enhanced therapeutic potential (*11*–*15*) and developing cell engineering strategies for improving efficacy (*8*). DCs stimulated by danger signals up-regulate costimulatory molecules that are essential for eliciting T cell–mediated immune responses (*16*, *17*); thus, leveraging costimulation-competent DCs is paramount for effective clinical applications. Various maturation cocktails have been used in clinical settings to induce desirable DC activation states, with promising outcomes observed in selected trials (*8*, *18*).

Traditional DC preparations typically involve patient-derived DCs—generally monocyte-derived DCs (moDCs)—loaded ex vivo with defined TAAs or patient-derived tumor lysates. This procedure is then followed by a maturation step aimed to promote DC activation, antigen presentation, and costimulation (*7*, *9*). An alternative approach involves enforcing the acquisition of TAAs by the adoptive transfer of DCs directly in the body of a patient with cancer (*8*). In this regard, tumor-derived extracellular vesicles (EVs), which circulate in the blood and through the lymphatic system, provide a source of relevant TAAs in patients with cancer (*19*). In pursuit of this, we previously developed DCs engineered to express a nonsignaling chimeric receptor, called EV-internalizing receptor (EVIR), which enhances the uptake of tumor-derived EVs displaying a known, cancer-specific surface molecule (referred to as the "bait molecule"). Upon binding of the EVIR's single-chain antibody fragment (scFv) to the bait molecule, the EVIR facilitates EV internalization and

[1]Swiss Institute for Experimental Cancer Research (ISREC), School of Life Sciences, Swiss Federal Institute of Technology in Lausanne (EPFL), 1015 Lausanne, Switzerland. [2]Agora Cancer Research Center, 1011 Lausanne, Switzerland. [3]Swiss Cancer Center Léman (SCCL), Switzerland. [4]Laboratory of the Physics of Biological Systems, Institute of Physics, EPFL, 1015 Lausanne, Switzerland. [5]Division of Pulmonary Medicine, Department of Medicine, Lausanne University Hospital (CHUV) and University of Lausanne (UNIL), 1011 Lausanne, Switzerland. [6]Division of Oncology, Department of Internal Medicine, Medical University of Graz, 8036 Graz, Austria. [7]Translational Data Science (TDS) Facility, Swiss Institute of Bioinformatics (SIB), 1011 Lausanne, Switzerland. [8]Department of Oncology, UNIL and CHUV, 1011 Lausanne, Switzerland. [9]Ludwig Institute for Cancer Research, Lausanne Branch, 1011 Lausanne, Switzerland.
†Present address: Novigenix SA, Epalinges, Switzerland.
*Corresponding author. Email: michele.depalma@epfl.ch

subsequent presentation of a wide range of TAAs, termed "prey antigens," found inside or on the surface of the EVs (*20*). We found that priming of T cells by EVIR-engineered DCs occurred largely through "cross-dressing," a process related to trogocytosis whereby preformed, membrane-associated major histocompatibility class I (MHCI)–peptide complexes are horizontally transferred from the cancer cells to the DCs via tumor-derived EVs, rather than being cross-presented on endogenous MHCI (*21*–*24*). These preformed antigen complexes may include immunologically relevant TAAs. However, the EVIR platform is potentially limited by a lack of bona fide cross-presentation of EV-associated TAAs (*20*). This limitation stems from the EVIR backbone, which is based on a truncated form of the low-affinity nerve growth factor receptor (ΔLNGFR) and lacks the intracellular signaling domains necessary to coordinate EV uptake with DC activation. Here, we describe a next-generation signaling EVIR, termed instructive chimeric antigen receptor (iCAR), which couples DC internalization of tumor-derived EVs with the acquisition of cross-dressing and cross-presentation capacities, resulting in enhanced T cell stimulatory activity.

RESULTS

Screening of signaling CARs identifies constructs that induce DC activation upon binding a surface cancer molecule

To develop a CAR capable of inducing DC activation upon ligand engagement, we used transmembrane receptors that naturally promote DC activation. Pattern recognition receptors (PRRs) can induce DC maturation upon binding to pathogen-associated molecular patterns, and among PRRs, C-type lectin receptors (CLRs) are broadly expressed in and can activate DCs and macrophages (*25*–*27*). We selected the CLRs DEC205 (also known as CD205), DC-SIGN (also known as CD209), DECTIN1 (also known as CLEC7A), CLEC9A, and MRC1 (also known as CD206) and replaced their extracellular ligand binding domains with an anti-human HER2 scFv. The new CLR-based CARs were named after their receptor backbones (e.g., DEC205-CAR). In addition to CLRs, CD40, Fc-gamma receptors (FcγRs), and FLT3 also induce DC activation upon ligand binding. We, therefore, generated CARs on the basis of these receptors (CD40-CAR, FcγRIV-CAR, and FLT3-CAR, respectively). We then transduced the cDC1-like MutuDC cell line (*28*) with lentiviral vectors (LVs) expressing the new signaling CARs, the nonsignaling EVIR based on ΔLNGFR (EVIR hereon), or a control receptor lacking the scFv domain (Ctrl-EVIR) and used NGFR or Fab antibodies to examine EVIR or CAR expression 2 days posttransduction. Although all receptors were efficiently expressed, expression varied with the individual construct (Fig. 1A).

To test the ability of signaling CARs to induce DC activation upon binding to a surface tumor molecule, we used MC38 colorectal cancer cells modified to express human HER2 (MC38-HER2; fig. S1A). We cocultured transduced DCs with MC38-HER2 cells at a 1:2 ratio for 12 hours. Expression of CD86, a costimulatory molecule involved in T cell activation (*29*), served as a readout for DC activation. As expected, the Ctrl-EVIR and the nonsignaling EVIR did not induce DC activation upon coculture with MC38-HER2 cells (Fig. 1B and fig. S1B). Among signaling CARs, DEC205-CAR, CLEC9A-CAR, DC-SIGN-CAR, MRC1-CAR, and FLT3-CAR failed to robustly activate the DCs. Three signaling CARs activated the DCs. However, DECTIN1-CAR–expressing DCs exhibited high CD86 expression both in the presence and absence of MC38-HER2 cells, indicative of tonic (ligand-independent) signaling of the CAR. Conversely, both CD40-CAR and FcγRIV-CAR up-regulated CD86 in DCs only upon coculture with MC38-HER2 cells, thus providing suitable CARs for further engineering.

An iCAR integrates antigen binding and DC activation while avoiding tonic signaling

We next sought to exploit the properties of both CD40-CAR and FcγRIV-CAR to develop an improved signaling CAR with antigen-binding–dependent DC activation capability. We noted that expression of the FcγRIV-CAR was relatively low in transduced DCs (see Fig. 1A above). Because FcγRs require assembly with the FcRγ chain for both trafficking to the cell surface and signaling (*30*), lentivirally expressed FcγRIV-CAR might compete with endogenous FcγRs for assembly with FcRγ chains, thus limiting surface expression of the exogenous FcγRIV-CAR. We then combined the intracellular CD40 activation domain of the CD40-CAR with the ITAM (immunoreceptor tyrosine-based activation motif) of the FcRγ chain in the same CAR. In addition, we substituted the CD40 transmembrane/hinge domain with a mutated (Cys^{193} to Ser^{193}) CD8a transmembrane/hinge domain. The mutated CD8a domain disrupts spontaneous (ligand-independent) dimerization/multimerization of the chimeric receptor to limit potential tonic signaling (*31*, *32*). The resultant signaling CAR encompasses (i) the anti-HER2 scFv extracellular domain, (ii) the mutated CD8a transmembrane/hinge domain, (iii) the CD40 activation domain, and (iv) the FcRγ chain ITAM and is here referred to as mutCD8/CD40-FcRγ-ITAM-CAR or iCAR for brevity (Fig. 1C).

We then transduced MutuDCs with the nonsignaling EVIR or the signaling iCAR and used an anti-Fab antibody to examine receptor expression. Both receptors showed robust and comparable expression at day 2 posttransduction (Fig. 1D). We then examined whether the iCAR could induce DC activation upon binding to HER2 presented by either MC38-HER2 cancer cells or their EVs. To this aim, we measured expression of CD86, C-C chemokine receptor type 7 (CCR7; involved in DC migration) (*33*), MHCII (involved in antigen presentation) (*34*), and CD40 (a costimulatory receptor involved in DC activation) (*35*) in the transduced DCs 12 hours after exposure to $HER2^+$ EVs or cancer cells. The iCAR robustly up-regulated the aforementioned markers in the presence of $HER2^+$ EVs or cancer cells (but not HER2-negative EVs or cancer cells), whereas the EVIR did not exhibit this capacity (Fig. 1E and fig. S2A). The iCAR did not up-regulate DC activation markers when the cells were left untreated or exposed to $HER2^-$ EVs or cancer cells, indicating the absence of tonic signaling and its proficiency in ligand-dependent signaling.

An anti-GD2 iCAR promotes DC activation in response to $GD2^+$ EVs

To demonstrate the versatility of the iCAR, we tested a second bait molecule. GD2 is a disialoganglioside preferentially expressed in some solid tumors, including neuroblastoma, glioma, lung cancer, and melanoma (*36*). GD2-targeted therapies, such as monoclonal antibodies and CAR T cells, have shown promise and safety for cancer treatment because of the limited expression of GD2 in normal tissues (*13*, *37*, *38*). We generated an anti-GD2 iCAR using a scFv domain previously used in the design of a nonsignaling EVIR (*20*). We modified an ovalbumin (OVA)–positive B16F10 melanoma cell line (B16F10-OVA) to express GD2 by transducing the GD2 synthases GD2S and GD3S, as described previously (*20*), and obtained

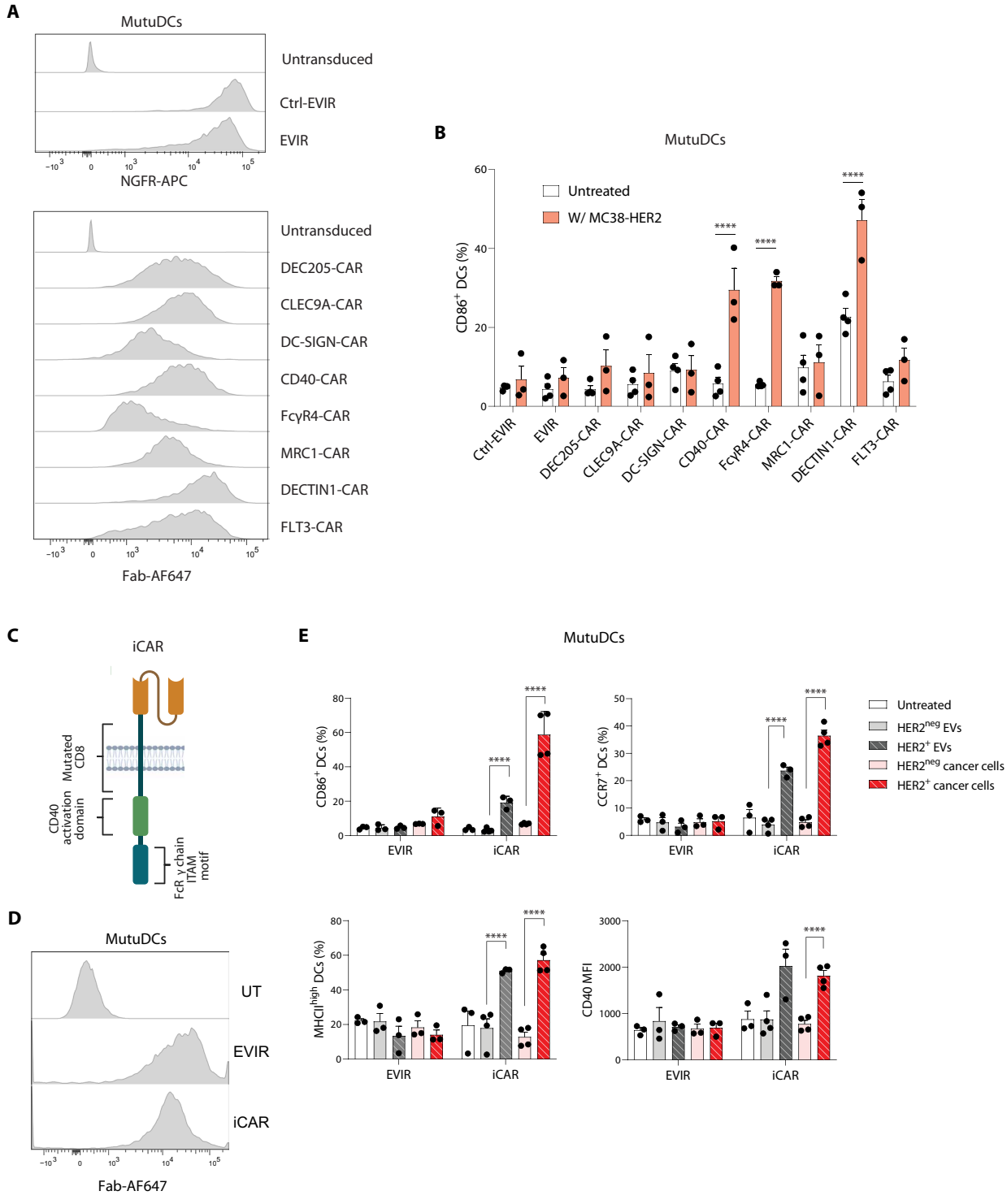

Fig. 1. An iCAR integrates antigen binding and DC activation while avoiding tonic signaling. (**A**) Flow cytometry analysis of the expression of the Crtl-EVIR, EVIR, and anti-HER2 CARs in MutuDCs using either anti-NGFR (top) or anti-Fab staining (bottom). A representative experiment is shown. (**B**) Flow cytometry analysis of CD86 in transduced MutuDCs 2 days after coculture with cancer cells (with MC38-HER2; $n = 3$) or left untreated ($n = 4$). Statistical analysis by one-way ANOVA with Šidák's correction for multiple comparisons. (**C**) Schematic representation of the iCAR design, created in BioRender. (**D**) Surface expression of anti-HER2 iCAR measured by anti-Fab flow cytometry analysis. UT, untransduced. (**E**) Flow cytometry analysis of activation markers in transduced MutuDCs treated as indicated (mean ± SEM; $n = 3$ independent cell cultures except for $HER2^{neg}$ or $HER2^{+}$ cancer cells with iCAR-DCs and $HER2^{neg}$ EVs with iCAR-DCs, where $n = 4$). MFI, mean fluorescence intensity. Statistical analysis by one-way ANOVA with Tukey's correction for multiple comparisons (only relevant comparisons are shown). ****$P < 0.0001$.

B16F10-GD2/OVA cells (fig. S3A). MutuDCs transduced with a Ctrl-iCAR (lacking the scFv domain) or anti-GD2 iCAR (Fig. 2A) were then exposed to $GD2^+$ EVs isolated from B16F10-GD2/OVA cells and analyzed 12 hours later. The EVs up-regulated CD86 and MHCII in iCAR but not Ctrl-iCAR–expressing DCs (Fig. 2, B and C). In addition, iCAR-DCs secreted higher amounts of T cell chemoattractants and stimulatory cytokines, such as CXCL10, CXCL9, interleukin-6 (IL-6), tumor necrosis factor–α (TNFα), and IL-12p40, in response to EVs, as compared with DCs expressing the Ctrl-iCAR (Fig. 2D). This response was enhanced by addition of interferon-γ (IFN-γ) to the cell culture medium. Under the same experimental conditions, lipopolysaccharide (LPS)—a danger-associated signal for DCs—up-regulated the expression of the aforementioned molecules to a greater extent than melanoma-derived EVs, consistent with its potent proinflammatory effects on DCs (fig. S3, B and C).

To broaden the characterization of iCAR-induced responses in DCs, we conducted bulk RNA sequencing (RNA-seq) of MutuDCs expressing either the iCAR or Ctrl-iCAR, after exposure to $GD2^+$ EVs or no treatment (Fig. 2E). In Ctrl-iCAR–DCs, EV exposure did not significantly alter the expression of individual genes; however, it globally down-regulated multiple inflammation-related gene pathways, including TNFα, IFN-α, and IFN-γ pathways (Fig. 2F and fig. S3D). This is consistent with the potentially immunosuppressive and tolerogenic properties of tumor-derived EVs (*39*–*43*). Conversely, the EVs robustly altered gene expression and elicited proinflammatory responses in iCAR-DCs (Fig. 2, G to I, and fig. S3E). Multiple classic DC activation and proinflammatory genes were up-regulated, including *Cd40*, *Cd80*, *Tnfsf7* (CD70), *Ms4a7*, *Tnfsf9* (4-1BBL), and *Icosl* (costimulatory molecules); *Il1b*, *Il6*, *Tnf*, *Il12b*, and *Il27* (proinflammatory cytokines); *Cxcl9* and *Cxcl10* (T cell chemoattractants); *Ccr7*; *Rel*, *Relb*, and *Nod2* [nuclear factor κB (NF-κB) pathway]; *Oas1a*, *Oas2*, *Oas3*, *Irf1*, and *Stat1* (IFN regulatory factors); and *B2m* and *H2* (antigen presentation molecules). We also observed up-regulation of genes implicated in DC maturation (*44*, *45*), such as *Cd274* [programmed death-ligand 1 (PD-L1)], a negative immune checkpoint. Gene set enrichment analysis with Hallmark revealed up-regulation of both type I and II IFN signaling, TNFα signaling via NF-κB, IL-6/Janus kinase/signal transducer and activator of transcription 3 signaling, and additional inflammation and immune-response pathways (e.g., inflammatory response and allograft rejection), among the most regulated pathways in iCAR-DCs exposed to EVs. Together, these data further illustrate GD2-specific DC activation mediated by the iCAR. Moreover, they indicate that the iCAR reverses the potentially suppressive signals deployed by tumor EVs to DCs to enforce, rather than blunt, their activation.

The iCAR promotes bait molecule–dependent DC activation conducive to T cell activation

We next asked whether iCAR-DCs promote T cell proliferation and activation in response to bait molecule–positive EVs. We used MutuDCs transduced with the Ctrl-iCAR, anti-HER2 iCAR, or the nonsignaling anti-HER2 EVIR, along with EVs isolated from MC38-HER2 cells modified to express OVA (MC38-HER2/OVA) as a surrogate neoantigen for examining antigen-specific T cell responses (fig. S4A). We exposed transduced DCs to two different EV doses, corresponding to either 400 or 800 EVs per DC, for 2 hours before coculture with OVA-specific, MHCI-restricted $CD8^+$ T cells (OT-I cells). We examined T cell proliferation 3 days later and observed EV dose–dependent promotion of T cell proliferation, which was greater with the iCAR (Fig. 3A). This was associated with increased TNFα expression (Fig. 3B), indicative of T cell activation. Thus, the iCAR promotes T cell proliferation and activation more efficiently than a nonsignaling EVIR in response to environmental EVs.

Activation of DCs is required for efficient antigen cross-presentation (*46*, *47*). We then asked whether DCs duly activated by the iCAR can cross-present TAAs to T cells. For this purpose, we used an *H2kb* (MHCI) knockout ($H2kb^{KO}$) MC38-HER2/OVA cell line (fig. S4A) (*20*). Because these cancer cells lack endogenous MHCI molecules, they cannot transfer preformed peptide-MHCI complexes (p-MHCI) to DCs through cross-dressing, an antigen presentation modality involving horizontal transfer of p-MHCI to antigen-presenting cells via EVs or trogocytosis (*21*). We previously showed that nonsignaling EVIRs facilitate DC presentation of TAAs through cross-dressing but not cross-presentation (*20*). We then cocultured transduced MutuDCs with $H2kb^{KO}$ MC38-HER2/OVA cells and $CD8^+$ OT-I cells and measured T cell proliferation 3 days later. As shown in Fig. 3C, the iCAR—but not the EVIR—stimulated OT-I cell proliferation under conditions of impaired cross-dressing, indicating that activation occurred via bona fide cross-presentation.

In addition to antigen presentation to $CD8^+$ T cells through MHCI, DCs can prime naïve $CD4^+$ T cells by presenting peptides loaded onto MHCII molecules (*21*). Because iCAR engagement by EVs or cancer cells up-regulated MHCII expression and IL-12p40 secretion in DCs, we asked whether iCAR-expressing MutuDCs could stimulate $CD4^+$ T cell proliferation and IFN-γ production in a coculture assay with MC38-HER2/OVA cells and $CD4^+$ OVA-specific, MHCII-restricted T cells (OT-II cells). Similar to results obtained with OT-I cells, the iCAR enhanced T cell proliferation (Fig. 3D) and IFN-γ expression (Fig. 3E) after 5 days of coculture, compared with the nonsignaling EVIR. Together, these data indicate that the iCAR endows DCs with the ability to acquire TAAs from cancer cells and present them to both $CD8^+$ and $CD4^+$ T cells, including via bona fide cross-presentation, in the absence of other exogenous stimuli.

iCAR-DCs sensitize murine melanoma to PD-1 blockade without the need for antigen loading

The B16F10 melanoma model is characterized by scant T cell infiltrates, low immunogenicity, and refractoriness to PD-1 blockade (*13*, *48*–*50*). We used this model to investigate the therapeutic potential of anti-GD2 iCAR-DCs in combination with a PD-1 blocking antibody.

In a first study, we examined whether iCAR-DCs would sensitize established tumors (>100 mm^3) to PD-1 blockade in a late intervention setting. We injected B16F10-GD2/OVA cells subcutaneously in mice and, on days 11 and 14 after tumor injection, intravenously administered 2×10^6 MutuDCs transduced with either Ctrl-iCAR or iCAR, along with PD-1 antibodies or irrelevant immunoglobulin Gs (IgGs; fig. S5A). We monitored tumor growth until day 18. In this setting, iCAR- but not Ctrl-iCAR–expressing DCs moderately delayed tumor growth in combination with PD-1 blockade (fig. S5B). This response required a combination of the iCAR and PD-1 antibodies, given that neither treatment alone had antitumoral activity in this late treatment setting.

In a second study, we treated the tumors at an earlier stage of growth and used primary moDCs, which provide a more physiological and preclinically relevant source of DCs for treatment trials in

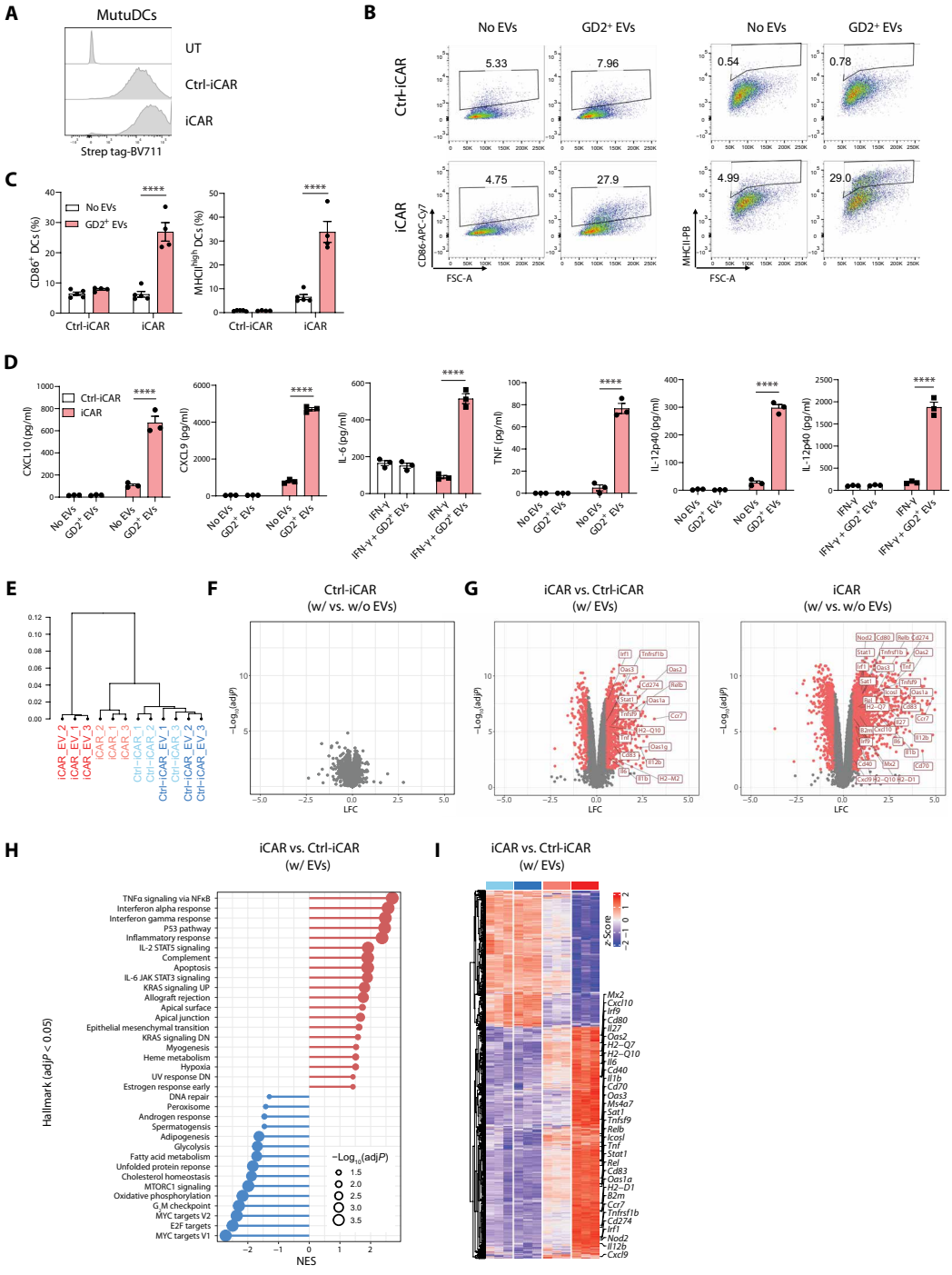

Fig. 2. An anti-GD2 iCAR promotes DC activation in response to GD2$^+$ EVs. (**A**) Flow cytometry analysis of the Ctrl-iCAR and anti-GD2 iCAR in MutuDCs, measured by anti-Fab staining. A representative experiment is shown. (**B** and **C**) Representative flow cytometry dot plots of CD86 (left) and MHCII (right) expression in MutuDCs transduced and treated as indicated (B), with quantification in (C) (mean ± SEM; $n = 5$ independent cell cultures for "no EVs" and $n = 4$ for GD2$^+$ EVs). Statistical analysis by one-way ANOVA with Tukey's correction for multiple comparisons (only relevant comparisons are shown). (**D**) Cytokine quantification in medium conditioned by MutuDCs transduced and treated as indicated (mean ± SEM; $n = 3$ independent cell cultures). Statistical analysis by one-way ANOVA with Tukey's correction for multiple comparisons (only relevant comparisons are shown). (**E** to **I**) Bulk RNA-seq analysis of MutuDCs transduced and treated as indicated ($n = 3$ independent cell cultures). (E) Clustering using an average method and Pearson correlation of the top 1000 most variable genes. [(F) and (G)] Volcano plots showing genes differentially expressed between MutuDCs transduced with Ctrl-iCAR and either treated with EVs or left untreated (F), MutuDCs either transduced with iCAR or Ctrl-iCAR and treated with EVs [(G), left], or MutuDCs transduced with iCAR and either treated with EVs or left untreated [(G), right]. Differentially expressed genes with adjusted $P < 0.05$ and $\log_2$(fold change) (LFC) < -0.5 or > 0.5 are shown in red. (H) Hallmark pathways significantly deregulated (adjusted $P < 0.05$) in the indicated comparison. NES, normalized enrichment score; UV, ultraviolet; UP, up-regulated; DN, down-regulated. (I) Heatmap of significantly changed genes (adjusted $P < 0.05$ and $-0.5 >$ LFC > 0.5) in the indicated comparisons. Color codes for the four comparison groups are like in (E). ****$P < 0.0001$. STAT5, signal transducer and activator of transcription 5; JAK, Janus kinase.

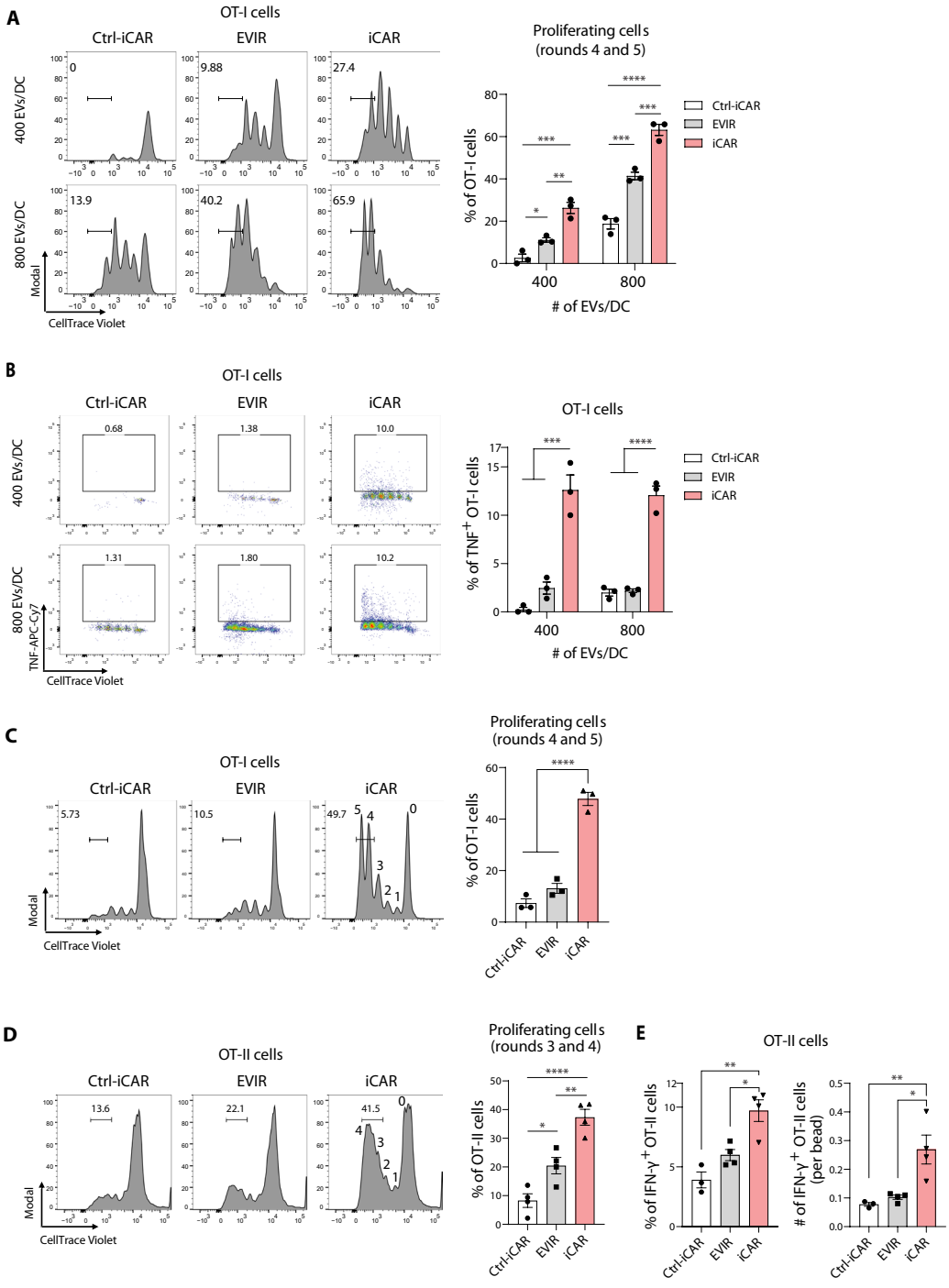

Fig. 3. iCAR promotes bait molecule–dependent DC activation conducive to T cell activation. (**A**) Flow cytometry analysis of OT-I cell proliferation in response to coculture with MutuDCs transduced and treated as indicated. Histogram plots on the left show peaks of T cell proliferation cycles revealed by dilution of CellTrace Violet; representative samples are shown. Quantification is shown on the right (mean ± SEM; $n = 3$ independent cell cultures). Statistical analysis by one-way ANOVA with Tukey's correction for multiple comparisons (conditions 400 and 800 were analyzed separately). (**B**) Flow cytometry analysis of intracellular TNF in OT-I cells cocultured with MutuDCs transduced and treated as indicated. Dot plots on the left show representative samples. Quantification is shown on the right (mean ± SEM; $n = 3$ independent cell cultures). Statistical analysis by one-way ANOVA with Tukey's correction for multiple comparisons (conditions 400 and 800 were analyzed separately). (**C** and **D**) Flow cytometry analysis of OT-I (C) or OT-II (D) cell proliferation in response to coculture with MutuDCs transduced as indicated and cocultured with *H2kb*^{KO} (C) or *H2kb*-proficient (D) MC38-HER2/OVA cells. Histogram plots on the left show peaks of T cell proliferation cycles revealed by dilution of CellTrace Violet; representative samples are shown. Quantification is shown on the right [mean ± SEM; $n = 3$ (C) or $n = 4$ (D) independent cell cultures]. Statistical analysis by one-way ANOVA with Tukey's correction for multiple comparisons. (**E**) Flow cytometry analysis of intracellular IFN-γ in OT-II cells cocultured with MutuDCs transduced as indicated and cocultured with MC38-HER2/OVA cells (mean ± SEM; $n = 3$ independent cell cultures for Ctrl-iCAR, and $n = 4$ for the other conditions). Statistical analysis by one-way ANOVA with Tukey's correction for multiple comparisons. $^*P < 0.05$, $^{**}P < 0.01$, $^{***}P < 0.001$, and $^{****}P < 0.0001$.

mice and patients with cancer (*7*). We injected B16F10-GD2/OVA cells subcutaneously in mice and, on days 7 and 9 after tumor injection, intravenously administered 2×10^6 moDCs transduced with either iCAR or Ctrl-iCAR, along with PD-1 antibodies (Fig. 4A). This dose regimen targets early-established tumors, which should allow sufficient time for the initiation of antitumor immunity by the engineered DCs. As shown in Fig. 4B, iCAR-moDCs delayed tumor growth compared with moDCs either untransduced or expressing the Ctrl-iCAR. Flow cytometry analysis of the tumors at the day 15 end point showed increased proportions of IFN-γ^+ or TNFα^+ CD8$^+$ and CD4$^+$ T cells in the tumors of some of the mice that received iCAR-moDCs (Fig. 4C). Higher proportions of IFN-γ^+ or TNFα^+ T cells in the tumors correlated with a better tumor response [compare samples in red in Fig. 4B (right) and Fig. 4C]. We did not observe counterselection of GD2$^+$ cancer cells in the tumors, which argues against the occurrence of iCAR-mediated selection of bait molecule–negative cancer clones (fig. S5C).

We next performed a survival study according to an early-intervention schedule (Fig. 4D). We terminated and censored the mice when the tumors surpassed a volume of 1000 mm^3. Consistent with the previous experiment, tumors of mice that received iCAR-moDCs exhibited, on average, delayed growth compared with the control group (Fig. 4, E and F), resulting in extended survival (Fig. 4G). Together, these results indicate that iCAR-DCs have antitumoral activity in an aggressive melanoma model without ex vivo antigen loading or concurrent cytoreductive therapy.

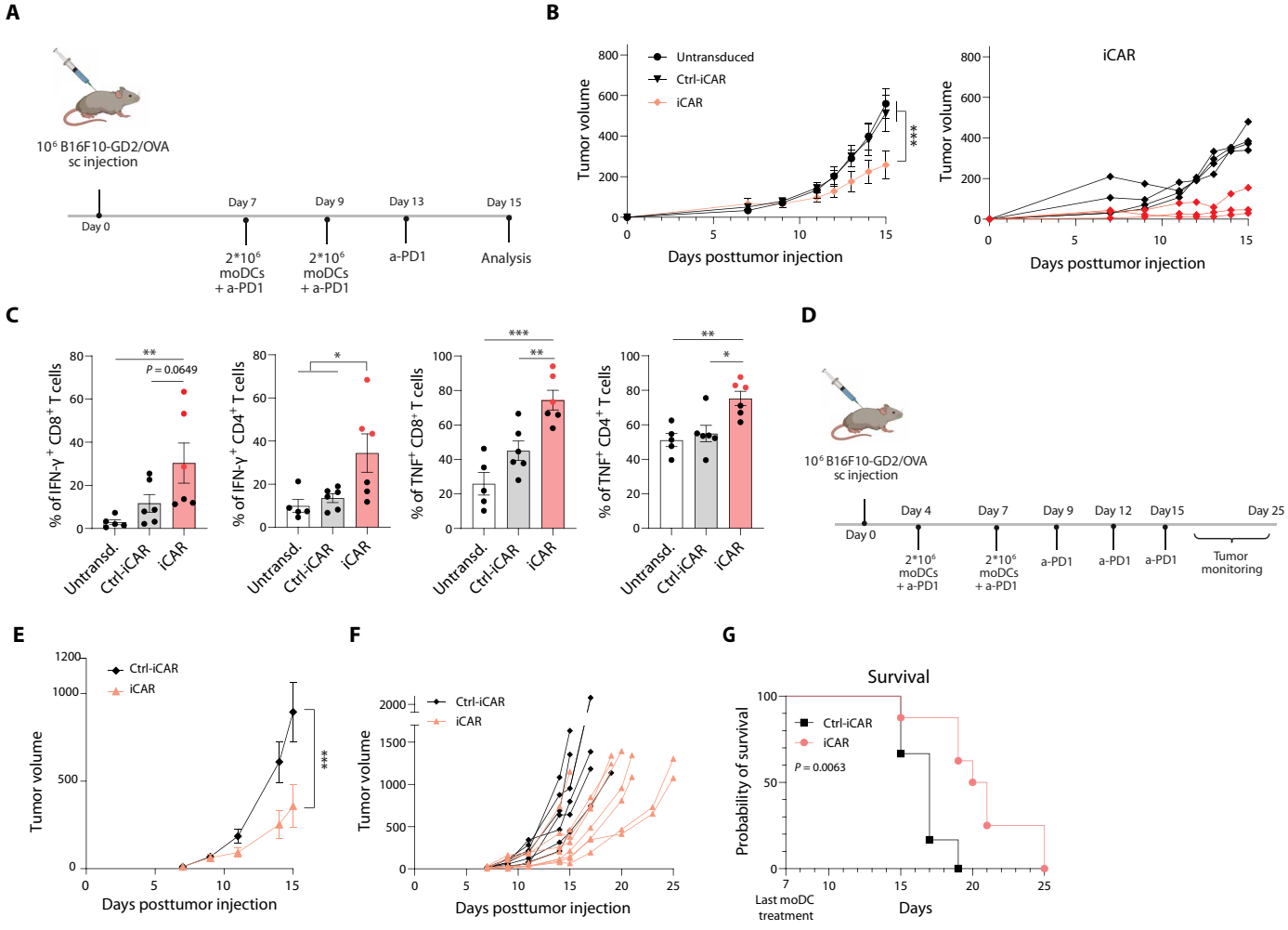

Fig. 4. iCAR-moDCs inhibit tumor growth without the need for antigen loading. (**A**) Schematic illustrating the experiment to study B16F10-GD2/OVA tumor response to the combination of a PD-1 antibody (a-PD1) and transduced moDCs; created in BioRender. (**B**) B16F10-GD2/OVA tumor growth. The graph on the left shows the tumor volumes (mean ± SEM; untransduced, $n = 5$; Ctrl-iCAR, $n = 6$; iCAR, $n = 7$) in mice treated as indicated. Statistical analysis by two-way ANOVA with Šidák's multiple comparisons test. The graph on the right shows the volumes of individual tumors in mice treated with iCAR-moDCs. (**C**) Flow cytometry analysis of intracellular IFN-γ and TNF in tumor-derived CD8$^+$ or CD4$^+$ T cells after ex vivo restimulation (mean ± SEM; untransduced, $n = 5$; Ctrl-iCAR, $n = 6$; iCAR, $n = 6$). Statistical analysis by one-way ANOVA with Tukey's correction for multiple comparisons. Samples in red indicate the three tumors in red in (B) above. (**D**) Schematic illustrating the experiment to study survival of mice bearing B16F10-GD2/OVA tumors and treated as indicated; created in BioRender. (**E**) B16F10-GD2/OVA tumor growth (mean volume ± SEM; Ctrl-iCAR, $n = 7$; iCAR, $n = 8$) shown until day 15 (time point when termination of the mice was initiated). Statistical analysis by two-way ANOVA with Šidák's multiple comparisons test. (**F**) Tumor growth in individual mice (Ctrl-iCAR, $n = 7$; iCAR, $n = 8$). (**G**) Survival analysis of mice treated as indicated (Ctrl-iCAR, $n = 6$; iCAR, $n = 8$). One mouse in the Ctrl-iCAR group was terminated before reaching the end point because of tumor necrosis. Statistical analysis by log-rank Mantel-Cox test. *$P < 0.05$, **$P < 0.01$, and ***$P < 0.001$.

A ubiquitination-resistant iCAR improves DC antigen cross-dressing and cross-presentation

Ubiquitination of transmembrane receptors after ligand engagement and signaling may direct them to the lysosome for degradation (*51*). To disrupt lysine ubiquitination of the anti-GD2 iCAR, we mutated all lysine residues into arginine in the intracellular receptor sequence. We termed the mutated receptor iCAR^{Ub} (Fig. 5A). By suppressing sorting to the lysosome/proteasome (*52*), impaired iCAR ubiquitination should increase both its stability at the cell surface and its recycling to the cell surface after internalization, thereby improving antigen presentation and, potentially, T cell priming.

MutuDCs transduced with the anti-GD2 iCAR^{Ub} showed robust surface expression of the receptor (Fig. 5B). In a cellular assay with MutuDCs exposed to PKH26-labeled EVs isolated from B16F10-GD2/OVA cells, iCAR^{Ub}-DCs exhibited increased EV internalization capacity compared with cells transduced with the iCAR or the nonsignaling EVIR (Fig. 5C). The ability of iCAR^{Ub}-DCs to efficiently internalize EVs was also associated with pronounced phagocytic activity in a cell coculture assay involving transduced moDCs and live B16F10-GD2/OVA cells prestained with a fluorescent, pH-sensitive dye (Fig. 5D). In this phagocytosis assay, however, moDCs expressing the unmodified iCAR also exhibited substantial phagocytic activity, almost matching that of iCAR^{Ub}-DCs.

We next asked whether the iCAR^{Ub} could enhance antigen presentation to CD8$^+$ T cells through cancer cell–derived EVs. We generated *B2m*^{KO} B16F10-GD2/OVA cells (which cannot present MHCI-restricted peptides) and performed an OT-I cell proliferation assay with transduced MutuDCs and two different doses of EVs derived from either *B2m*-proficient or *B2m*^{KO} B16F10-GD2/OVA cells. DCs expressing the iCAR^{Ub} were more efficient at inducing OT-I cell proliferation than cells transduced with the unmodified iCAR or a control, scFv-less ubiquitination-resistant receptor (Ctrl-iCAR^{Ub}), in response to *B2m*-proficient EVs (fig. S6A). Moreover, actively cycling T cells expressed higher TNFα in response to iCAR^{Ub}-DCs than cells transduced with other receptor constructs (fig. S6B). However, *B2m*^{KO} EVs failed to induce DC-dependent OT-I cell proliferation (fig. S6C) and TNFα expression (fig. S6D), regardless of the chimeric receptor used, indicating that T cell activation promoted by iCAR^{Ub}-DCs and *B2m*-proficient EVs occurred only through cross-dressing.

The aforementioned findings may seem to conflict with results in Fig. 3C above, in which *H2kb*^{KO} MC38-HER2/OVA cells conferred iCAR-expressing MutuDCs with the ability to activate OT-I cells via cross-presentation. However, the modality of antigen acquisition and presentation by DCs may vary with the source of the antigen (e.g., intact cancer cells versus EVs) and cell type (e.g., B16F10 versus MC38 cells) (*53*). Because tumor-derived EVs contain limiting amounts of soluble (full-length) OVA available for cross-presentation (*54*), we generated B16F10-GD2/OVA cells that coexpressed a membrane-bound form of OVA (mOVA) (B16F10-GD2/mOVA; fig. S6E). We then isolated EVs from *B2m*^{KO} B16F10-GD2/mOVA cells and assayed the ability of moDCs to activate OT-I cells in response to two different EV doses. Whereas both iCAR- and iCAR^{Ub}-moDCs failed to induce OT-I cell proliferation in response to *B2m*^{KO} EVs isolated from B16F10-GD2/OVA cells, they elicited T cell proliferation in response to *B2m*^{KO} EVs isolated from B16F10-GD2/mOVA cells (Fig. 5E). This effect was enhanced by the iCAR^{Ub}, especially at the lower EV dose. As expected, moDCs effectively induced OT-I cell proliferation in response to *B2m*-proficient EVs isolated from B16F10-GD2/OVA cells, an effect mediated through cross-dressing rather than cross-presentation (fig. S6F). Together, these results indicate that the iCAR—and especially an iCAR^{Ub} variant—can enforce DC presentation of an EV-associated tumor antigen through both cross-dressing and cross-presentation.

iCAR^{Ub}-moDCs elicit antigen-specific T cells in a murine melanoma model

We then examined whether iCAR^{Ub}-moDCs could elicit antigen-specific T cells in the absence of antigen loading. Mice carrying B16F10-GD2/OVA tumors (Fig. 6A) received a PD-1 antibody either with phosphate-buffered saline (PBS) or in combination with moDCs transduced with different chimeric receptors, including iCAR^{Ub} and other versions (Fig. 6B), on days 4 and 7. iCAR^{Ub}-moDCs delayed tumor growth compared with moDCs expressing a scFv-deficient iCAR^{Ub} (Fig. 6C). In this setting of antigen-agnostic DC therapy, iCAR^{Ub}-moDCs moderately enhanced the prevalence of CD8$^+$ T cells specific for TRP2 (an endogenous melanoma TAA) compared with the other chimeric receptors, an antigen-specific response that became more evident when both TRP2 and OVA-specific T cell populations were cumulatively assessed (Fig. 6D).

To further corroborate these results, we also performed a study with MC38-GD2 cells (fig. S7A). To delay tumor growth, which is otherwise very fast in this model, tumor-bearing mice received a single dose of cisplatin followed by PD-1 blockade in combination with moDCs transduced with different receptors, including iCAR^{Ub} and earlier versions, on days 14 and 17 (fig. S7B). We also treated a cohort of mice with moDCs pulsed ex vivo with a MC38-GD2 cell lysate, a procedure representative of traditional antigen loading of moDCs. Although all tumors progressed, iCAR^{Ub}-moDCs delayed tumor growth to a greater extent than moDCs transduced with other receptors or pulsed with the tumor lysate (fig. S7, C and D). This response was associated with a similar infiltration of CD8$^+$ T cells specific for P15E or REPS1, two MC38 tumor antigens, in tumors that received either tumor-pulsed moDCs or iCAR^{Ub}-moDCs (fig. S7E). These results suggest that the iCAR^{Ub} promotes DC presentation of TAAs to T cells, providing an alternative strategy to ex vivo DC pulsing with tumor lysates.

iCAR^{Ub}-moDC–regulated IL-12 inhibits tumor growth and increases T cell diversity in a poorly immunogenic melanoma model

We next explored whether iCAR signaling–dependent activation of moDCs could be exploited to transactivate an exogenous gene in an inducible fashion. To this end, we used a mutated *Il12* promoter (*55*) to regulate the expression of IL-12, a potent immunostimulatory cytokine (*56*). We performed double transduction of moDCs to codeliver the iCAR^{Ub} (or its scFv-deficient control) together with the inducible IL-12 expression cassette (Fig. 6E). In vitro, iCAR^{Ub}-moDCs—but not Ctrl-iCAR^{Ub}-moDCs—robustly up-regulated the secretion of IL-12 in response to coculture with B16F10-GD2 cells (fig. S7F).

We then tested the inducible platform in mice challenged with an OVA-negative B16F10 melanoma model. Mice bearing B16F10-GD2 tumors received moDCs transduced with either iCAR^{Ub} or Ctrl-iCAR^{Ub}, with or without the inducible IL-12 expression cassette, along with PD-1 antibodies on days 7, 10, and 13 (Fig. 6F). We also treated a cohort of mice with moDCs pulsed ex vivo with a B16F10-GD2 cell lysate. As shown in Fig. 6G, iCAR^{Ub}-moDCs—and to a greater extent

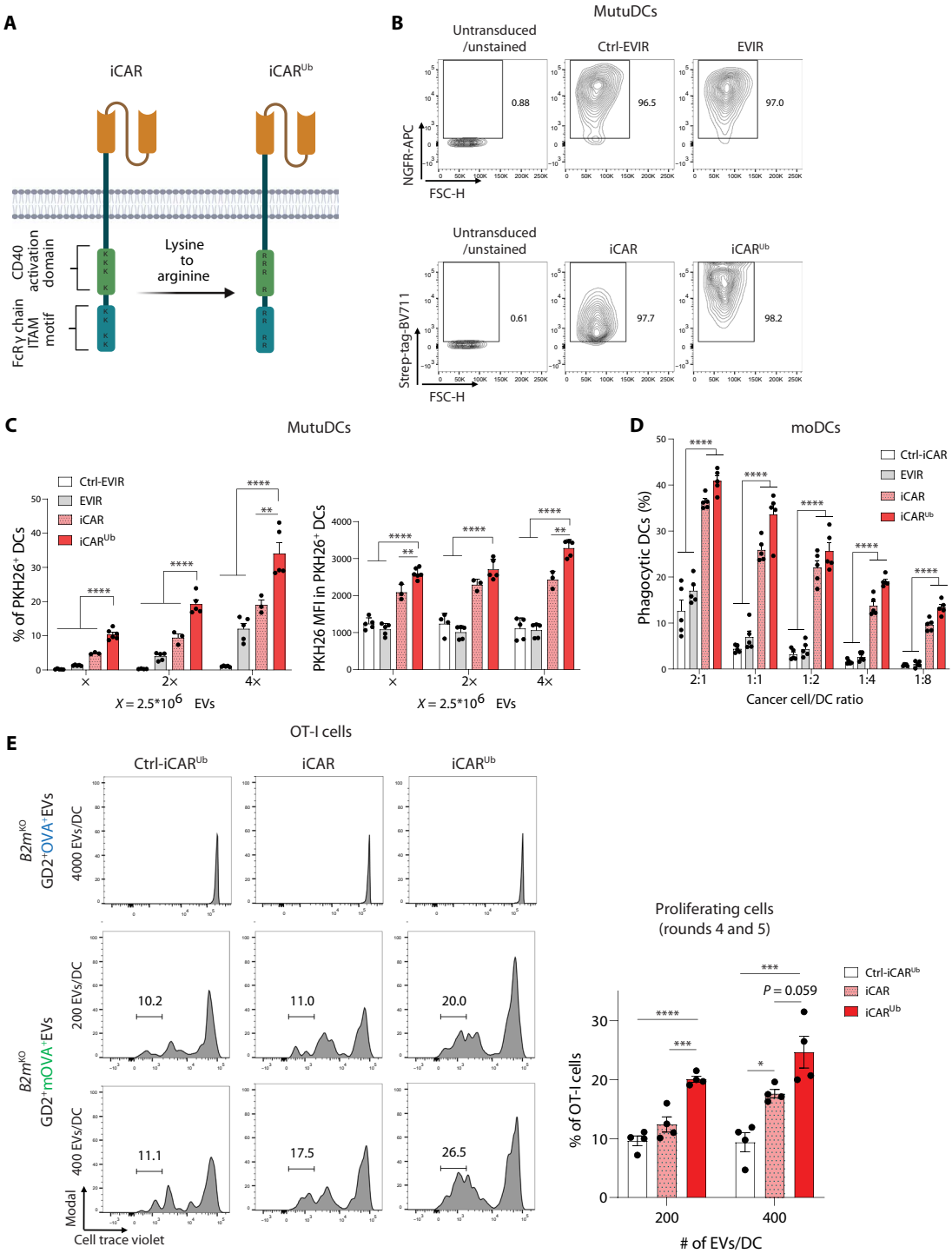

Fig. 5. A ubiquitination-resistant iCAR improves DC antigen cross-dressing and cross-presentation. (**A**) Schematic illustrating the iCAR^{Ub} design. (**B**) Flow cytometry analysis of the indicated anti-GD2 receptors in MutuDCs; representative samples are shown. (**C**) Flow cytometry analysis of PKH26 fluorescence in MutuDCs transduced and treated with labeled EVs as indicated [mean ± SEM; Ctrl-EVIR, $n = 4$ (EV dose 2×) or 5 (× and 4×); EVIR, $n = 5$; iCAR, $n = 3$; iCAR^{Ub}, $n = 5$ (2× and 4×) or 6 (×) independent cell cultures]. Statistical analysis by one-way ANOVA with Tukey's correction for multiple comparisons (only relevant comparisons are shown). (**D**) Flow cytometry analysis of phagocytic moDCs, revealed by pHrodo Red fluorescence. MoDCs transduced as indicated were cocultured with B16F10-GD2/OVA cells exposed to pHrodo Red (mean ± SEM; $n = 5$ independent cell cultures). Statistical analysis by one-way ANOVA with Tukey's correction for multiple comparisons. (**E**) Flow cytometry analysis of OT-I cell proliferation in response to coculture with moDCs transduced and treated with OVA$^+$ or mOVA$^+$ EVs as indicated. Histogram plots on the left show peaks of T cell proliferation cycles revealed by dilution of CellTrace Violet; representative samples are shown. Data on the right show T cells that performed four or five rounds of cell division (mean ± SEM; $n = 4$ independent cell cultures). Statistical analysis by one-way ANOVA with Tukey's correction for multiple comparisons. $^*P < 0.05$, $^{**}P < 0.01$, $^{***}P < 0.001$, and $^{****}P < 0.0001$.

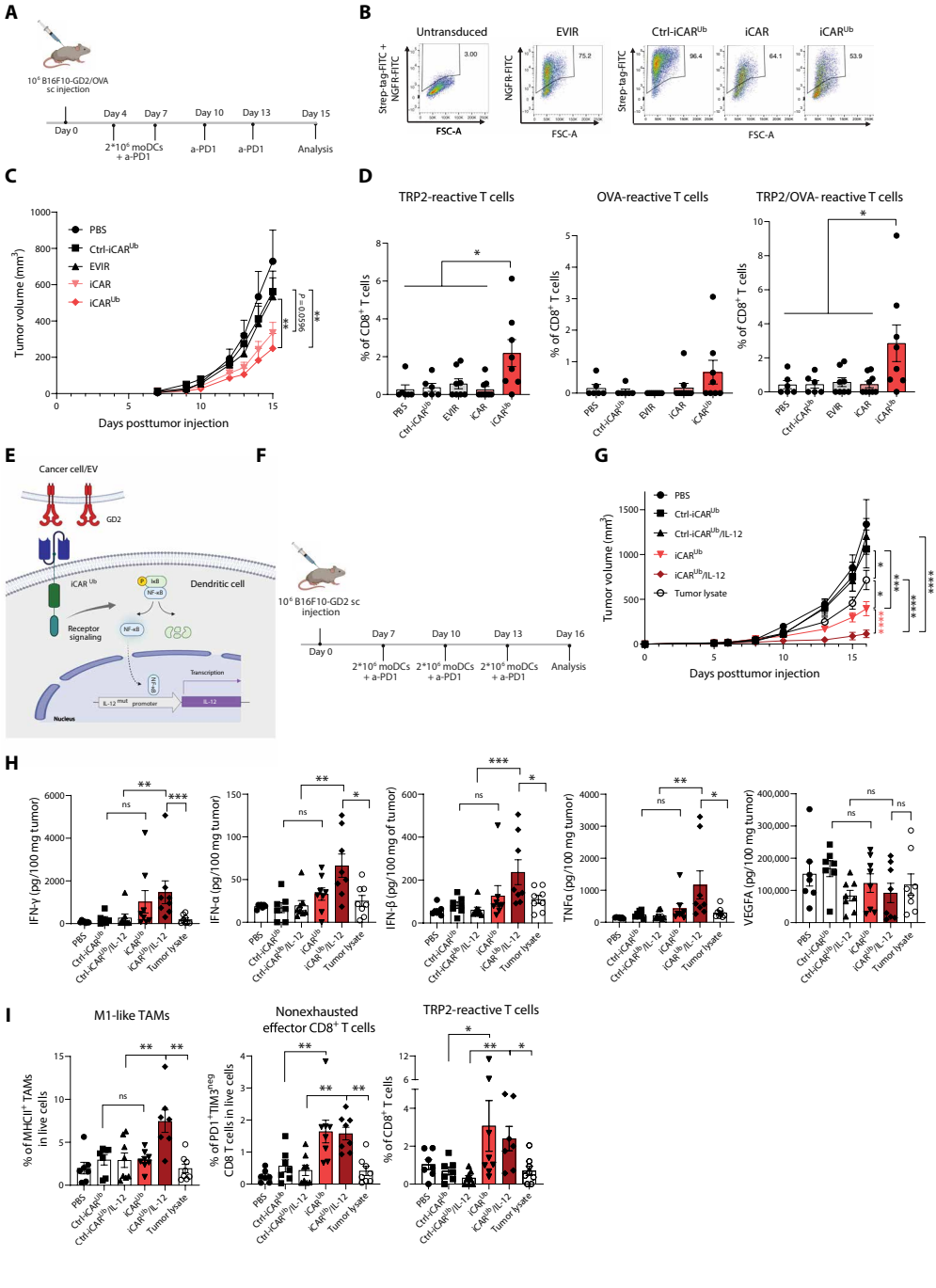

Fig. 6. iCAR^{Ub}-moDC–regulated IL-12 inhibits tumor growth in a poorly immunogenic melanoma model. (**A**) Schematic illustrating the experiment to study B16F10-GD2/OVA tumor response to transduced moDCs; created in BioRender. (**B**) Flow cytometry analysis of moDCs transduced as indicated. FITC, fluorescein isothiocyanate. (**C**) B16F10-GD2/OVA tumor growth. Data show tumor volumes (mean ± SEM; PBS, $n = 7$; Ctrl-iCAR^{Ub}, $n = 7$; EVIR, $n = 8$; iCAR, $n = 9$; iCAR^{Ub}, $n = 8$). Statistical analysis by two-way ANOVA with Šidák's multiple comparisons test. (**D**) Flow cytometry analysis by dextramer staining of TRP2 or OVA-reactive CD8$^+$ T cells (left and middle) or the combination of both (right), in tumors of mice treated as indicated (mean ± SEM; PBS, $n = 6$; Ctrl-iCAR^{Ub}, $n = 6$; EVIR, $n = 8$; iCAR, $n = 9$; iCAR^{Ub}, $n = 8$). Statistical analysis by one-way ANOVA with Tukey's correction for multiple comparisons. (**E**) Schematic of the inducible platform; created in BioRender. (**F**) Schematic illustrating the experiment to study the iCAR-inducible platform in the B16F10-GD2 model; created in BioRender. (**G**) B16F10-GD2 tumor growth. Data show tumor volumes (mean ± SEM; PBS, $n = 7$; Ctrl-iCAR^{Ub}, Ctrl-iCAR^{Ub}/IL-12, iCAR^{Ub}, iCAR^{Ub}/IL-12, and tumor lysate, $n = 8$). Statistical analysis by two-way ANOVA with Šidák's multiple comparisons test. The comparison between iCAR^{Ub}/IL-12 and iCAR^{Ub}, indicated with the red symbol, used two-way ANOVA with Šidák's multiple comparisons test performed between the two groups of interest. (**H**) Quantification of the indicated cytokines in the tumors of mice treated as indicated (mean ± SEM; PBS and Ctrl-iCAR^{Ub}, $n = 7$, except for IFN-γ in Ctrl-iCAR^{Ub}, where $n = 6$; Ctrl-iCAR^{Ub}/IL-12, iCAR^{Ub}, iCAR^{Ub}/IL-12, and tumor lysate, $n = 8$). Statistical analysis by two-tailed Mann-Whitney test comparing Ctrl-iCAR^{Ub} versus iCAR^{Ub}, Ctrl-iCAR^{Ub}/IL-12 versus iCAR^{Ub}/IL-12, and iCAR^{Ub}/IL-12 versus tumor lysate. (**I**) Flow cytometry analysis of MHCII$^+$ M1-like tumor-associated macrophages (TAMs) (mean ± SEM; PBS, Ctrl-iCAR^{Ub}, and iCAR^{Ub}/IL-12, $n = 7$; Ctrl-iCAR^{Ub}/IL-12, iCAR^{Ub}, and tumor lysate, $n = 8$), PD1$^+$TIM3^{neg} CD8$^+$ T cells (PBS and Ctrl-iCAR^{Ub}, $n = 7$; Ctrl-iCAR^{Ub}/IL-12, iCAR^{Ub}, iCAR^{Ub}/IL-12, and tumor lysate, $n = 8$), and TRP2 dextramer$^+$ CD8$^+$ T cells (PBS, Ctrl-iCAR^{Ub}, and iCAR^{Ub}/IL-12, $n = 7$; Ctrl-iCAR^{Ub}/IL-12, iCAR^{Ub}, and tumor lysate, $n = 8$) in the tumors of mice treated as indicated. Statistical analysis by two-tailed Mann-Whitney test comparing Ctrl-iCAR^{Ub} versus iCAR^{Ub}, Ctrl-iCAR^{Ub}/IL-12 versus iCAR^{Ub}/IL-12, and iCAR^{Ub}/IL-12 versus tumor lysate. *$P < 0.05$, **$P < 0.01$, ***$P < 0.001$, and ****$P < 0.0001$. ns, not significant.

iCAR^{Ub}/IL-12–moDCs—delayed tumor growth, whereas moDCs expressing the scFv-deficient receptor (with or without the inducible IL-12 cassette) failed to do so. Ex vivo pulsed moDCs had more limited efficacy than iCAR-moDCs in this OVA-negative model.

Although cytokine expression varied across independent tumors, iCAR^{Ub}/IL-12–moDCs up-regulated several proinflammatory cytokines, such as IFN-γ, IFN-α, IFN-β, and TNFα [but not immunosuppressive vascular-endothelial growth factor A (VEGFA)], compared with Ctrl-iCAR^{Ub}/IL-12–moDCs or moDCs pulsed with the cancer cell lysate (Fig. 6H and fig. S7G). This response was associated with a higher infiltration of MHCII$^+$ (M1-like) inflammatory macrophages. In addition, both iCAR^{Ub}-moDCs and iCAR^{Ub}/IL-12–moDCs moderately increased the proportions of nonexhausted (PD-1$^+$TIM3$^-$) and TRP2-specific CD8$^+$ T cells in the

tumors compared with moDCs expressing scFv-deficient receptors or pulsed with the cancer cell lysate (Fig. 6I and fig. S7H). These results suggest cooperative effects between iCAR^{Ub}-induced T cell responses and IL-12–dependent proinflammatory programming of the tumor microenvironment in a nonimmunogenic melanoma model.

To gain insight into T cell diversity, we performed bulk sequencing of T cell receptor β (TCRβ) in the tumors of mice that received moDCs, as described previously (*57*). The inherently low T cell numbers in B16F10 tumors, combined with the relatively small size of the tumors in mice that received iCAR^{Ub}- or iCAR^{Ub}/IL-12–moDCs, necessitated a pooled analysis (n = 8 mice per group). We found greater diversity in the T cell repertoire of tumors treated with iCAR^{Ub}- or iCAR^{Ub}/IL-12–moDCs, as shown by the overall higher number of unique clonotypes (Fig. 7A). In particular, we observed a higher relative abundance of low- and medium-frequency ("small" and "medium") clonotypes (Fig. 7B), which indicates diversification of the repertoire. This was also evidenced by higher D50 and 100X index values (Fig. 7, C and D). A higher D50 value is indicative of a more diverse TCR repertoire, given that a larger number of unique clonotypes contribute to half of the total TCR sequences (*58*). In addition, a higher D100X value is indicative of polyclonal diversification, being defined as the number of clonotypes whose frequency is at least 100-fold higher than the median clonotype frequency in that sample (*59*). Furthermore, tumors of mice treated with iCAR^{Ub}- or iCAR^{Ub}/IL-12–moDCs shared a higher proportion of clonotypes, indicative of potentially shared antigen-specific clones (Fig. 7E). The tumors of mice treated with ex vivo–loaded moDCs demonstrated a greater representation of hyperexpanded clonotypes at the expense of low- and medium-frequency clonotypes, which may be consistent with the ex vivo pulsing procedure. Although limited to a pooled analysis, these data further support the notion that iCAR-moDCs, particularly when incorporating an inducible IL-12 cassette, stimulate T cell responses even in poorly immunogenic tumors and without the need for ex vivo antigen loading.

Internalization of human melanoma EVs leads to iCAR-moDC activation

We humanized the anti-GD2 iCAR sequence and its scFv-deficient control (Ctrl-iCAR) for LV-mediated expression in human primary moDCs. Transduced human moDCs efficiently expressed the human iCAR, although the surface density of the iCAR appeared less than that of the Ctrl-iCAR, possibly because of less efficient transmembrane trafficking imposed by the scFv domain (Fig. 8A).

Although the anti-GD2 scFv of the iCAR binds GD2 of both murine and human origin (*36*), we sought to study EV internalization and DC activation in a fully human system to avoid potential xenogenic effects of the EVs on the human moDCs. To this aim, we screened several human melanoma cell lines (*60*) for the expression of GD2 and selected a GD2$^+$ cell line (T333A) and a GD2-negative cell line (T618A) for isolating EVs (Fig. 8B). As expected, GD2 was present on the surface of EVs isolated from GD2$^+$ but not GD2-negative melanoma cells (Fig. 8C). We then exposed both iCAR- and Ctrl-iCAR–moDCs to increasing amounts of PKH26-labeled EVs and examined EV internalization 2 hours later. iCAR-moDCs internalized the EVs in a dose-dependent manner and much more efficiently than Ctrl-iCAR–moDCs (Fig. 8, D and E).

We then asked whether GD2$^+$ EV internalization by iCAR-moDCs was conducive to DC activation. GD2$^+$ but not GD2-negative EVs enhanced the expression of CD86 (a costimulatory molecule not expressed in unstimulated moDCs) and HLA-DR (human leukocyte antigen-DR, a constitutively expressed moDC marker) in iCAR- but not Ctrl-iCAR–moDCs (Fig. 8, F and G, and fig. S8, A and B). These results provide initial functional validation of the iCAR platform in human moDCs.

DISCUSSION

Here, we described a signaling-competent CAR, called iCAR, developed for inducing DC activation and antigen presentation specifically in response to the recognition and acquisition of TAAs. Although

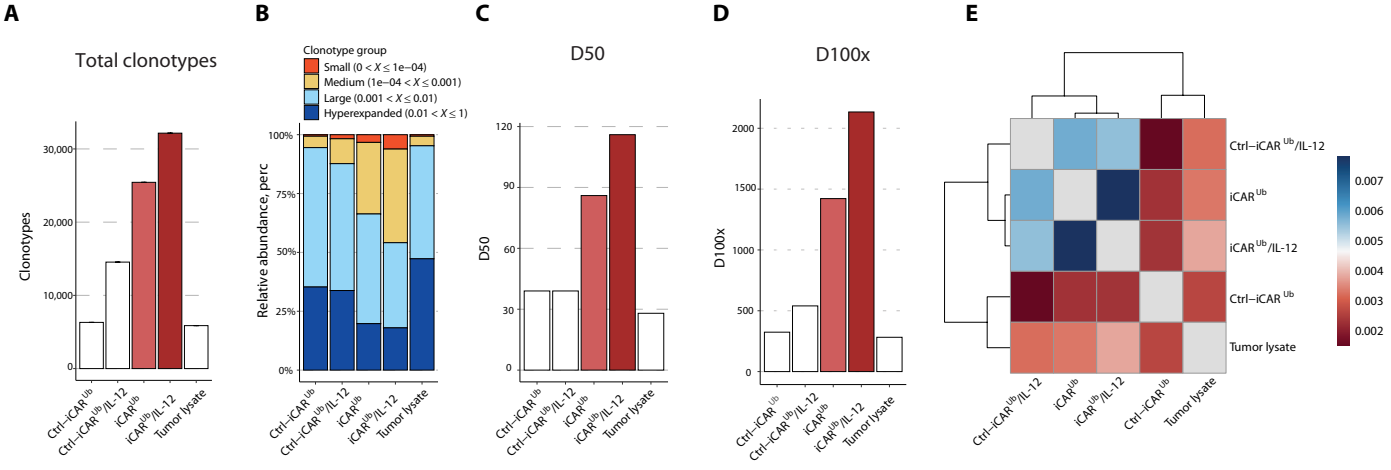

Fig. 7. iCAR^{Ub}-moDC–regulated IL-12 increases T cell diversity in a poorly immunogenic melanoma model. (**A**) Bar plot representation of the unique TCRβ clonotypes found in tumors of mice treated with moDCs expressing Ctrl-iCAR^{Ub}, Ctrl-iCAR^{Ub}/IL-12, iCAR^{Ub}, or iCAR^{Ub}/IL-12 or moDCs pulsed with tumor lysate (single replicate derived from pooled TCR sequences from all mice in each respective cohort). (**B**) Stacked bar plot representing the relative abundance in percentages (perc) of the clones that are hyperexpanded (frequency between 0.01 and 1), large (frequency between 0.001 and 0.01), medium (frequency between 0.0001 and 0.001), and small (frequency between 0 and 0.0001) in the full repertoire. (**C** and **D**) Bar plots of the diversity parameters, D50 and D100X. (**E**) Heatmap representing repertoire overlap measured using the Jaccard index.

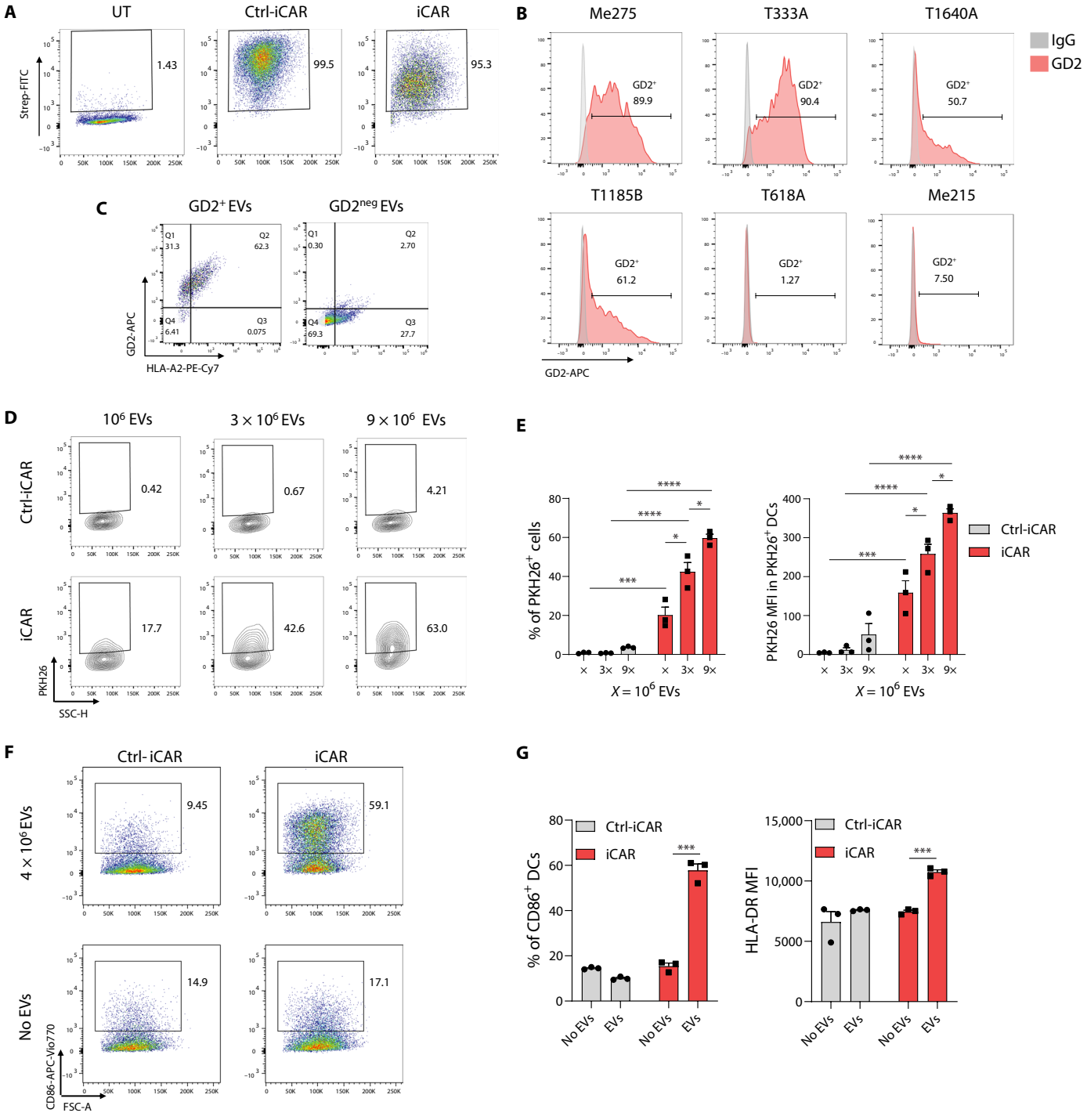

Fig. 8. Internalization of melanoma EVs leads to human iCAR-moDC activation. (**A**) Flow cytometry analysis of the indicated receptors in transduced human moDCs. Representative samples are shown. (**B**) Flow cytometry analysis of GD2 expression in human melanoma cell lines. Representative samples are shown. (**C**) Flow cytometry analysis of GD2 expression in EVs isolated from either GD2-positive (T333A) or GD2-negative (T618A) human melanoma cell lines. Representative samples are shown. (**D** and **E**) Flow cytometry analysis of EV uptake by human moDCs transduced with the indicated receptors and treated with the indicated doses of $GD2^+$ EVs derived from the T333A human melanoma cell line. (D) Representative samples; (E) quantification of the data (mean ± SEM, $n = 3$ replicates from one donor). Statistical analysis by one-way ANOVA with Tukey's correction for multiple comparisons (only relevant comparisons are shown). (**F** and **G**) Flow cytometry analysis of the indicated activation markers in human moDCs expressing the indicated receptors, treated with $GD2^+$ EVs derived from T333A human melanoma cell line. (F) Representative flow cytometry plots; (G) quantification of the data (mean ± SEM, $n = 3$ replicates from one donor). Statistical analysis by unpaired two-tailed Student's t test (only relevant comparisons are shown). $^*P < 0.05$, $^{***}P < 0.001$, and $^{****}P < 0.0001$.

CARs were originally designed for engineering lymphoid cells, there have been efforts to express these signaling chimeric receptors also in myeloid cells, such as macrophages (*61*–*63*). A CAR for directing human macrophages to HER2$^+$ cancer involved an anti-HER2 scFv and a CD3ζ intracellular domain, also used for traditional CAR T cells (*62*). These CAR macrophages were shown to phagocytose cancer cells in vitro and to inhibit the growth of HER2$^+$ tumors in mice. Another macrophage CAR design used an intracellular CD3ζ sequence linked to the Toll/interleukin 1 receptor (TIR) domain of TLR4, equivalent to a second-generation CAR (*63*). Addition of the TIR domain prompted CAR macrophage acquisition of an M1-like (tumoricidal and immunostimulatory) phenotype, which improved cytotoxicity toward cancer cells in vitro and tumor control in mice. Additional CAR macrophage designs were developed that used intracellular fragments of CD28, FcεR1γ, TLR4, IFNGR1, or IFNGR2 (*64*). Potential limitations of CAR macrophages are their limited ability to traffic to tumors upon intravascular administration and their suboptimal antigen presentation capacity, shortcomings that may contribute to explain the lack of sustained responses in an early clinical trial (*65*).

The extracellular scFv domain of the iCAR endows the DCs with the ability to internalize tumor-derived membrane particles (e.g., EVs) or phagocytose cancer cells that display on their surface the bait molecule recognized by the scFv (e.g., HER2 or GD2). This process is conducive to the presentation by the DC of TAAs contained in the internalized tumor material (called prey antigens). The iCAR coordinates acquisition of TAAs and activation of the DC. iCAR-expressing DCs undergo activation specifically in response to contact with bait molecule–positive EVs or cancer cells, as shown by the up-regulation of DC activation/maturation markers (including antigen presentation, costimulatory, and promigratory molecules) and cytokine secretion (including T cell chemoattractants). In addition, bulk RNA-seq analysis of iCAR-DCs treated with GD2$^+$ melanoma–derived EVs revealed iCAR-dependent acquisition of an activated DC phenotype characterized by up-regulated type I and II IFN signatures. We also found that melanoma-derived EVs suppressed, rather than enhanced, some immunostimulatory pathways in control DCs—a response that was reversed by the iCAR. Similarly, human iCAR-moDCs efficiently internalized GD2$^+$ human melanoma–derived EVs, a response that was associated with activation of the DCs. Coordinate acquisition of TAAs and activation of the iCAR-DCs are biologically relevant, given that antigen acquisition must be followed by proper activation of the DC for achieving efficient T cell priming (*47*, *66*–*69*). Our observation that GD2$^+$ EVs triggered a milder DC activation and cytokine secretion response compared with LPS may be beneficial for DC functionality, potentially by reducing the risk of early exhaustion or functional impairment that might occur in response to potent danger-associated signals (*67*).

The iCAR differs substantially from the first-generation EVIR we developed previously (*20*). The EVIR was based on a truncated, nonsignaling NGFR receptor and, therefore, lacked the ability to relay activation signals in the DC. Compared with a nonsignaling anti-GD2 EVIR, the signaling-competent iCAR conferred the DCs with improved EV internalization and cancer cell phagocytosis capabilities. The observed increase in EV uptake and cancer cell phagocytosis is likely due to signals deployed from the FcRγ chain ITAM of the iCAR. It is known that FcγRs direct internalization of opsonized cells and pathogens through FcRγ chain signaling (*70*). Accordingly, mutation of the ITAM in the FcRγ chain was shown to disrupt uptake of opsonized particles by DCs (*71*). Also, the iCAR promoted more robust OT-I and OT-II cell proliferation and cytokine production—indicative of superior T cell priming capacity—than the nonsignaling EVIR. This enhancement may be due to both improved antigen uptake and delivery of costimulatory signals and proinflammatory cytokines to T cells by iCAR-DCs. The use of *H2kb*/*B2m*-proficient or *H2kb*/*B2m*-deficient cancer cells revealed that iCAR-DCs can present an MHCI-restricted surrogate neoantigen to T cells via both cross-dressing and cross-presentation, whereas nonsignaling EVIRs lacked the latter property (*20*).

In many signaling pathways, internalization and subsequent ubiquitination and degradation of the signaling receptor provide a negative feedback mechanism that attenuates signaling. For instance, the CD3-TCR complex undergoes rapid internalization upon TCR engagement, and subsequent CD3ζ ubiquitination leads to the degradation of the complex, which limits TCR signaling (*51*). To enforce iCAR expression and function, we modified it by mutating all lysine residues to arginine. Arginine does not get ubiquitinated but has a positive charge similar to lysine; thus, the mutations are unlikely to affect the structural properties of the iCAR. We termed the modified receptor iCAR^{Ub} and observed an increase in iCAR^{Ub} surface expression compared with the parental iCAR, suggesting improved stability. The anti-GD2 iCAR^{Ub} also moderately enhanced the uptake of GD2$^+$ EVs and, in T cell proliferation assays, demonstrated improved cross-presentation and cross-dressing capacity compared with cells expressing the unmodified iCAR. These results suggest that ubiquitination resistance may endow the iCAR with improved performance in future cell therapy applications.

iCAR-DCs inhibited the growth of B16F10 melanoma, which is unresponsive to immune checkpoint blockade with PD-1 or PD-L1 antibodies (*13*, *48*–*50*, *72*). In a B16F10 model lacking artificial neoantigens, iCAR-DCs increased TRP2-specific T cells and expanded the TCR repertoire, especially by increasing the representation of low-frequency clonotypes. At variance with CAR T cells, which directly eliminate antigen-positive cancer cell clones (*3*–*5*), iCAR-DCs should promote polyclonal T cell responses not conducive to antigen-negative clonal selection. Expansion of CD8$^+$ T cells against B16F10 TAAs raised the intriguing possibility that iCAR-DCs may promote epitope spreading (*73*) in treated mice. These effects are achieved without the need for ex vivo antigen loading or intratumoral administration of the DCs, demonstrating an antigen-agnostic mechanism operative in immunosuppressive tumor microenvironments.

We exploited iCAR-induced up-regulation of endogenous IL-12 to design an inducible system encompassing a mutated *Il12* promoter (*74*, *75*). Transactivation of the mutated *Il12* promoter through iCAR signaling enabled the coordinate expression of a second transgene. Our data indicate that this platform can be used to enforce expression of a therapeutic cytokine, IL-12, further improving tumor control in a nonimmunogenic B16F10 melanoma model. In the future, the iCAR-based inducible platform may be used for enhancing TAA acquisition and presentation while targeting the delivery of potent and otherwise potentially toxic cytokines to the tumor microenvironment.

Our study is not without limitations. Although we demonstrated that iCAR-DCs can present an EV- or cancer cell–associated surrogate antigen to both CD8$^+$ and CD4$^+$ T cells in vitro, the precise modalities of antigen presentation in tumor-bearing mice remain unknown. Specifically, it is unclear whether these cells activate antitumor immune responses in secondary lymphoid organs (such as

tumor-draining lymph nodes), in the tumor microenvironment, or both. Future studies should investigate these dynamics and their kinetics to inform the optimization of dosage regimens. Furthermore, although biological sensitivity was observed, the treatment did not induce substantial tumor regression or prolonged disease stabilization in the B16F10 melanoma model. Prior studies have reported more pronounced antitumor responses in this model (*76*). For example, one study achieved effective tumor eradication through the combination of four immunotherapies: recombinant IL-2 with extended half-life, anti–PD-1, active vaccination against the highly immunogenic TRP2 TAA, and a TRP2-targeting antibody (*76*). It should be noted, however, that iCAR-moDCs delayed tumor growth without the need for vaccination with defined immunogenic TAAs or administration of recombinant cytokines. Moreover, iCAR-moDCs were superior to moDCs pulsed ex vivo with cancer cell lysates in controlling tumor growth and eliciting tumor-specific T cells. This suggests that iCAR-DCs may obviate the need for DC loading and maturation steps (*7*), offering a tumor and antigen-agnostic approach that does not depend on prior knowledge or availability of TAAs or patient-derived material.

In the future, iCAR-moDCs may be combined with strategies that mobilize tumor-derived EVs, such as certain cytoreductive treatments (*77*), to increase the pool of TAAs available for uptake and presentation. In addition, these engineered DCs could be integrated with complementary immunotherapies that enhance or synergize with DC-mediated antigen presentation (*8*), further amplifying the antitumor immune response.

MATERIALS AND METHODS

Study design

This study was designed to develop and therapeutically deploy a platform of CARs capable of promoting the selective uptake of TAAs by DCs while simultaneously enhancing their activation. To achieve this, we initially screened a panel of CAR constructs and identified a lead candidate, termed iCAR, which we characterized using the MutuDC line under standardized conditions (Figs. 1 to 3). We then evaluated the mode of action and therapeutic potential of engineered DCs in adoptive transfer experiments in tumor-bearing mice, primarily using primary moDCs and OVA-expressing B16F10 melanoma models (Fig. 4). Subsequently, we developed a refined, ubiquitination-resistant variant of iCAR, termed iCAR^{Ub}, capable of transactivating IL-12 upon binding to GD2. We then tested its efficacy in mice bearing GD2-positive B16F10 melanomas, including OVA-negative variants, to assess both therapeutic activity and immune responses (Figs. 5 to 7). Last, we generated human primary iCAR-moDCs to demonstrate their capacity for selective uptake of GD2-positive EVs derived from human GD2-positive melanoma cells (Fig. 8).

No statistical methods were used to calculate the sample size. In each experiment involving murine or human DC cultures, studies were carried out with a minimum of three independent replicates per condition (i.e., cell cultures were transduced and treated independently). Mouse experiments were performed once. However, independent replicate mouse studies were conducted under similar experimental conditions and included some overlapping control groups. These independent studies yielded consistent results, supporting the reproducibility of the findings. In experiments involving tumor-bearing mice treated with systemic DC administrations, five to nine mice per condition were used, and two or three subsequent doses of DCs were administered intravenously via the tail vein. DCs were injected when tumors were either palpable and measurable or palpable but not yet measurable; detailed timelines for each experiment are shown in the figures and figure legends. Tumor size was measured with calipers, and tumor volume was calculated using the formula $0.5 \times d^2 \times D$, where "d" is the shorter and "D" is the longer tumor diameter. Mice were monitored three times per week to assess general health. In the survival study, mice were terminated when tumor volume reached 1000 mm^3. In other studies, which focused on examining changes in lymphoid immune cells in the tumor as well as therapeutic effects, all mice were scheduled for termination at fixed end points before or when tumors in vehicle (control)–treated mice reached 1000 mm^3 in volume.

In mouse studies, to mitigate variability across cages, each cage contained at least one mouse from every treatment group. For randomization, in experiments where DCs were injected into mice with palpable tumors, animals were allocated to treatment groups such that average tumor sizes were similar across cohorts. Tumor volumes were measured in a blinded manner by trained technical staff (although investigators had access to mouse IDs on a separate spreadsheet), and no outliers were excluded from the analyses. Investigators were not blinded when analyzing flow cytometry or cytokine expression data. Mice, and biological samples derived from them, were occasionally removed from the studies based on one of the following criteria: (i) absence of a detectable or measurable tumor at the time of randomization; (ii) development of tumor necrosis or inflammation likely to affect tumor growth or immune infiltration; or (iii) insufficient quantity or unacceptable quality of the sample after processing and preparation for analysis, such as flow cytometry.

End points for mouse experiments were selected in accordance with institutionally approved criteria. All animal studies were conducted in compliance with protocols approved by the Veterinary Authorities of the Canton of Vaud in accordance with Swiss law (protocols VD3154, VD3154.1, and VD3785). Detailed information on sample sizes and statistical methods is provided in the figure legends.

Mouse studies

Eight- to 12-week-old female C57BL/6 mice (Charles River) were used for tumor studies. All mice were maintained under specific pathogen–free conditions at the EPFL or Agora animal facility in Lausanne, Switzerland. Mice were housed in individually ventilated cages with a 12-hour light/dark cycle.

Cancer cells were thawed and cultured for at least 1 week before subcutaneous injection in mice. The cells were split 1 day before injection to achieve ~70% confluency on the day of injection, ensuring that they were in their exponential growth phase. We inoculated 0.5×10^6 MC38-GD2, 1×10^6 B16F10-GD2, or 1×10^6 B16F10-GD2/OVA cancer cells in 100 μl of PBS subcutaneously in the right flank.

For all experiments involving systemic DC administration, two or three subsequent doses of 2×10^6 DCs were administered intravenously (via the tail vein) in tumor-bearing mice. In some experiments, DCs were injected when tumors were palpable and growing, whereas in others, they were injected when tumors were detectable but not yet measurable; detailed timelines for each experiment are shown in the figures.

Tumor-bearing mice received intraperitoneal injections of either anti-PD1 antibody (10 mg/kg; rat IgG2a, clone RMPI-14, Bio X Cell

InvivoMAb, catalog no. BE0146) or an isotype rat IgG2a (10 mg/kg; clone 2A3, Bio X Cell InvivoMAb, catalog no. BE0089), in 100 μl of PBS, at the intervals shown in the figures. Additional information is provided in the "Study design" section here and in the Supplementary Materials.

Statistical analysis and reproducibility

GraphPad Prism software was used to generate graphs and perform statistical analyses. For each experiment involving murine or human DC cultures, comparisons between two groups with normally distributed variables were analyzed using a two-tailed, unpaired Student's *t* test. When comparisons involved more than two groups, one-way analysis of variance (ANOVA) with correction for multiple comparisons was applied. The specific statistical test used in each experiment is reported in the figure legends.

To examine differences in tumor volume over time, two-way ANOVA with post hoc correction for multiple comparisons (as defined in the figure legends) was used. In one instance, two-way ANOVA was also applied to compare two specific groups within a larger dataset; in this case, statistical significance between the two groups is indicated by an additional red symbol (Fig. 6G). In the survival study, a log-rank (Mantel-Cox) test was used to compare mouse cohorts. For comparisons of tumor parameters (such as immune cell infiltrates) across multiple experimental groups, one-way ANOVA with post hoc correction for multiple comparisons (defined in the figure legends) was the preferred statistical test. In cases where the measured parameter exhibited substantial intersample variability (such as intratumoral cytokine concentrations), a two-tailed Mann-Whitney test was used to compare specific groups of interest (e.g., iCAR^{Ub} versus Ctrl-iCAR^{Ub}). The statistical test used in each mouse experiment is specified in the corresponding figure legend.

Error bars represent the SEM. Statistical significance of the data is indicated as follows: $*P < 0.05$, $**P < 0.01$, $***P < 0.001$, and $****P < 0.0001$.

Supplementary Materials

This PDF file includes:

Materials and Methods
Figs. S1 to S8
Legend for table S1
Legend for data file S1
References (*78*–*81*)

Other Supplementary Material for this manuscript includes the following:

Table S1
Data file S1
MDAR Reproducibility Checklist

REFERENCES AND NOTES

1. Q. Sun, Z. Hong, C. Zhang, L. Wang, Z. Han, D. Ma, Immune checkpoint therapy for solid tumours: Clinical dilemmas and future trends. *Signal Transduct. Target. Ther.* **8**, 320 (2023).
2. A. D. Waldman, J. M. Fritz, M. J. Lenardo, A guide to cancer immunotherapy: From T cell basic science to clinical practice. *Nat. Rev. Immunol.* **20**, 651–668 (2020).
3. M. Morotti, A. Albukhari, A. Alsaadi, M. Artibani, J. D. Brenton, S. M. Curbishley, T. Dong, M. L. Dustin, Z. Hu, N. McGranahan, M. L. Miller, L. Santana-Gonzalez, L. W. Seymour, T. Shi, P. Van Loo, C. Yau, H. White, N. Wietek, D. N. Church, D. C. Wedge, A. A. Ahmed, Promises and challenges of adoptive T-cell therapies for solid tumours. *Br. J. Cancer* **124**, 1759–1776 (2021).
4. K. K. Patel, M. Tariveranmoshabad, S. Kadu, N. Shobaki, C. June, From concept to cure: The evolution of CAR-T cell therapy. *Mol. Ther.* **33**, 2123–2140 (2025).
5. U. Uslu, C. H. June, Beyond the blood: Expanding CAR T cell therapy to solid tumors. *Nat. Biotechnol.* **43**, 506–515 (2025).
6. M. Saxena, S. Balan, V. Roudko, N. Bhardwaj, Towards superior dendritic-cell vaccines for. *Nat. Biomed. Eng.* **2**, 341–346 (2018).
7. A. Harari, M. Graciotti, M. Bassani-Sternberg, L. E. Kandalaft, Antitumour dendritic cell vaccination in a priming and boosting approach. *Nat. Rev. Drug Discov.* **19**, 635–652 (2020).
8. C. R. Perez, M. De Palma, Engineering dendritic cell vaccines to improve cancer immunotherapy. *Nat. Commun.* **10**, 5408 (2019).
9. I. Heras-Murillo, I. Adán-Barrientos, M. Galán, S. K. Wculek, D. Sancho, Dendritic cells as orchestrators of anticancer immunity and immunotherapy. *Nat. Rev. Clin. Oncol.* **21**, 257–277 (2024).
10. L. M. Liau, K. Ashkan, S. Brem, J. L. Campian, J. E. Trusheim, F. M. Iwamoto, D. D. Tran, G. Ansstas, C. S. Cobbs, J. A. Heth, M. E. Salacz, S. D'Andre, R. D. Aiken, Y. A. Moshel, J. Y. Nam, C. P. Pillainayagam, S. A. Wagner, K. A. Walter, R. Chaudhary, S. A. Goldlust, I. Y. Lee, D. A. Bota, H. Elinzano, J. Grewal, K. Lillehei, T. Mikkelsen, T. Walbert, S. Abram, A. J. Brenner, M. G. Ewend, S. Khagi, D. S. Lovick, J. Portnow, L. Kim, W. G. Loudon, N. L. Martinez, R. C. Thompson, D. E. Avigan, K. L. Fink, F. J. Geoffroy, P. Giglio, O. Gligich, D. Krex, S. M. Lindhorst, J. Lutzky, H. J. Meisel, M. Nadji-Ohl, L. Sanchin, A. Sloan, L. P. Taylor, J. K. Wu, E. M. Dunbar, A. B. Etame, S. Kesari, D. Mathieu, D. E. Piccioni, D. S. Baskin, M. Lacroix, S. A. May, P. Z. New, T. J. Pluard, S. A. Toms, V. Tse, S. Peak, J. L. Villano, J. D. Battiste, P. J. Mulholland, M. L. Pearlman, K. Petrecca, M. Schulder, R. M. Prins, A. L. Boynton, M. L. Bosch, Association of autologous tumor lysate-loaded dendritic cell vaccination with extension of survival among patients with newly diagnosed and recurrent glioblastoma: A phase 3 prospective externally controlled cohort trial. *JAMA Oncol.* **9**, 112–121 (2023).
11. S. S. Hernández, M. R. Jakobsen, R. O. Bak, Plasmacytoid dendritic cells as a novel cell-based cancer immunotherapy. *Int. J. Mol. Sci.* **23**, 11397 (2022).
12. K. F. Bol, G. Schreibelt, K. Rabold, S. K. Wculek, J. K. Schwarze, A. Dzionek, A. Teijeira, L. E. Kandalaft, P. Romero, G. Coukos, B. Neyns, D. Sancho, I. Melero, I. J. M. De Vries, The clinical application of cancer immunotherapy based on naturally circulating dendritic cells. *J. Immunother. Cancer* **7**, 109 (2019).
13. A. Ghasemi, A. Martinez-Usatorre, L. Li, M. Hicham, A. Guichard, R. Marcone, N. Fournier, B. Torchia, D. Martinez Bedoya, S. Davanture, M. Fernández-Vaquero, C. Fan, J. Janzen, Y. Mohammadzadeh, R. Genolet, N. Mansouri, M. Wenes, D. Migliorini, M. Heikenwalder, M. De Palma, Cytokine-armed dendritic cell progenitors for antigen-agnostic cancer immunotherapy. *Nat. Cancer* **5**, 240–261 (2024).
14. H. Westdorp, J. H. A. Creemers, I. M. Van Oort, G. Schreibelt, M. A. J. Gorris, N. Mehra, M. Simons, A. L. De Goede, M. M. Van Rossum, A. J. Croockewit, C. G. Figdor, J. A. Witjes, E. H. J. G. Aarntzen, R. D. M. Mus, M. Brüning, K. Petry, M. Gotthardt, J. O. Barentsz, I. J. M. De Vries, W. R. Gerritsen, Blood-derived dendritic cell vaccinations induce immune responses that correlate with clinical outcome in patients with chemo-naive castration-resistant prostate cancer. *J. Immunother. Cancer* **7**, 302 (2019).
15. K. Lenogue, A. Walencik, K. Laulagnier, J. P. Molens, H. Benlalam, B. Dreno, P. Coulie, M. Pule, L. Chaperot, J. Plumas, Engineering a human plasmacytoid dendritic cell-based vaccine to prime and expand multispecific viral and tumor antigen-specific t-cells. *Vaccine* **9**, 141 (2021).
16. S. K. Wculek, F. J. Cueto, A. M. Mujal, I. Melero, M. F. Krummel, D. Sancho, Dendritic cells in cancer immunology and immunotherapy. *Nat. Rev. Immunol.* **20**, 7–24 (2020).
17. C. Goyvaerts, K. Breckpot, The journey of in vivo virus engineered dendritic cells from bench to bedside: A bumpy road. *Front. Immunol.* **9**, 2052 (2018).
18. Y. Gu, X. Zhao, X. Song, Ex vivo pulsed dendritic cell vaccination against cancer. *Acta Pharmacol. Sin.* **41**, 959–969 (2020).
19. J. Wolfers, A. Lozier, G. Raposo, A. Regnault, C. Théry, C. Masurier, C. Flament, S. Pouzieux, F. Faure, T. Tursz, E. Angevin, S. Amigorena, L. Zitvogel, Tumor-derived exosomes are a source of shared tumor rejection antigens for CTL cross-priming. *Nat. Med.* **7**, 297–303 (2001).
20. M. L. Squadrito, C. Cianciaruso, S. K. Hansen, M. De Palma, EVIR: Chimeric receptors that enhance dendritic cell cross-dressing with tumor antigens. *Nat. Methods* **15**, 183–186 (2018).
21. A. Martinez-Usatorre, M. De Palma, Dendritic cell cross-dressing and tumor immunity. *EMBO Mol. Med.* **14**, e16523 (2022).
22. B. P. Dolan, K. D. Gibbs, S. Ostrand-Rosenberg, Dendritic cells cross-dressed with peptide MHC class I complexes prime CD8$^+$ T cells. *J. Immunol.* **177**, 6018–6024 (2006).
23. V. Russo, D. Zhou, C. Sartirana, P. Rovere, A. Villa, S. Rossini, C. Traversari, C. Bordignon, Acquisition of intact allogeneic human leukocyte antigen molecules by human dendritic cells. *Blood* **95**, 3473–3477 (2000).
24. M. Zagorulya, S. Spranger, Once upon a prime: DCs shape cancer immunity. *Trends Cancer* **9**, 172–184 (2023).
25. D. Sancho, C. R. e Sousa, Signaling by myeloid C-Type lectin receptors in immunity and homeostasis. *Annu. Rev. Immunol.* **30**, 491–529 (2012).
26. T. B. H. Geijtenbeek, S. I. Gringhuis, Signalling through C-type lectin receptors: Shaping immune responses. *Nat. Rev. Immunol.* **9**, 465–479 (2009).
27. M. Scur, B. D. Parsons, S. Dey, A. P. Makrigiannis, The diverse roles of C-type lectin-like receptors in immunity. *Front. Immunol.* **14**, 1126043 (2023).

28. S. A. Fuertes Marraco, F. Grosjean, A. Duval, M. Rosa, C. Lavanchy, D. Ashok, S. Haller, L. A. Otten, Q. G. Steiner, P. Descombes, C. A. Luber, F. Meissner, M. Mann, L. Szeles, W. Reith, H. Acha-Orbea, Novel murine dendritic cell lines: A powerful auxiliary tool for dendritic cell research. *Front. Immunol.* **3**, 331 (2012).
29. I. J. Thomas, L. G. Petrich de Marquesini, R. Ravanan, R. M. Smith, S. Guerder, R. A. Flavell, D. C. Wraith, L. Wen, F. S. Wong, CD86 has sustained costimulatory effects on CD8 T cells. *J. Immunol.* **179**, 5936–5946 (2007).
30. M. K. Kim, Z. Y. Huang, P. H. Hwang, B. A. Jones, N. Sato, S. Hunter, T. H. Kim-Han, R. G. Worth, Z. K. Indik, A. D. Schreiber, Fcγ receptor transmembrane domains: Role in cell surface expression, γ chain interaction, and phagocytosis. *Blood* **101**, 4479–4484 (2003).
31. S. Hennecke, P. Cosson, Role of transmembrane domains in assembly and intracellular transport of the CD8 molecule. *J. Biol. Chem.* **268**, 26607–26612 (1993).
32. C. Beppler, J. Eichorst, K. Marchuk, E. Cai, C. A. Castellanos, V. Sriram, K. T. Roybal, M. F. Krummel, Hyperstabilization of T cell microvilli contacts by chimeric antigen receptors. *J. Cell Biol.* **222**, e202205118 (2023).
33. J. Liu, X. Zhang, Y. Cheng, X. Cao, Dendritic cell migration in inflammation and immunity. *Cell. Mol. Immunol.* **18**, 2461–2471 (2021).
34. P. A. Roche, K. Furuta, The ins and outs of MHC class II-mediated antigen processing and presentation. *Nat. Rev. Immunol.* **15**, 203–216 (2015).
35. T. N. J. Bullock, CD40 stimulation as a molecular adjuvant for cancer vaccines and other immunotherapies. *Cell. Mol. Immunol.* **19**, 14–22 (2022).
36. P. Machy, E. Mortier, S. Birklé, Biology of GD2 ganglioside: Implications for cancer immunotherapy. *Front. Pharmacol.* **14**, 1249929 (2023).
37. F. Del Bufalo, B. De Angelis, I. Caruana, G. Del Baldo, M. A. De Ioris, A. Serra, A. Mastronuzzi, M. G. Cefalo, D. Pagliara, M. Amicucci, G. Li Pira, G. Leone, V. Bertaina, M. Sinibaldi, S. Di Cecca, M. Guercio, Z. Abbaszadeh, L. Iaffaldano, M. Gunetti, S. Iacovelli, R. Bugianesi, S. Macchia, M. Algeri, P. Merli, F. Galaverna, R. Abbas, M. C. Garganese, M. F. Villani, G. S. Colafati, F. Bonetti, M. Rabusin, K. Perruccio, V. Folsi, C. Quintarelli, F. Locatelli, GD2-CART01 for relapsed or refractory high-risk neuroblastoma. *N. Engl. J. Med.* **388**, 1284–1295 (2023).
38. B. Nazha, C. Inal, T. K. Owonikoko, Disialoganglioside GD2 expression in solid tumors and role as a target for cancer therapy. *Front. Oncol.* **10**, 1000 (2020).
39. V. Fleming, X. Hu, C. Weller, R. Weber, C. Groth, Z. Riester, L. Hüser, Q. Sun, V. Nagibin, C. Kirschning, V. Bronte, J. Utikal, P. Altevogt, V. Umansky, Melanoma extracellular vesicles generate immunosuppressive myeloid cells by upregulating PD-L1 via TLR4 signaling. *Cancer Res.* **79**, 4715–4728 (2019).
40. S. Raimondo, M. Pucci, R. Alessandro, S. Fontana, Extracellular vesicles and tumor-immune escape: Biological functions and clinical perspectives. *Int. J. Mol. Sci.* **21**, 2286 (2020).
41. C. Yang, S. H. Kim, N. R. Bianco, P. D. Robbins, Tumor-derived exosomes confer antigen-specific immunosuppression in a murine delayed-type hypersensitivity model. *PLOS ONE* **6**, e22517 (2011).
42. T. L. Whiteside, Exosomes and tumor-mediated immune suppression. *J. Clin. Invest.* **126**, 1216–1223 (2016).
43. F. Cocozza, L. Martin-Jaular, L. Lippens, A. D. Cicco, Y. A. Arribas, N. Ansart, F. Dingli, M. Richard, L. Merle, M. J. S. Roman, P. Poullet, D. Loew, D. Lévy, A. Hendrix, G. Kassiotis, A. Joliot, M. Tkach, C. Théry, Extracellular vesicles and co-isolated endogenous retroviruses from murine cancer cells differentially affect dendritic cells. *EMBO J.* **42**, e113590 (2023).
44. K. Abdi, N. J. Singh, P. Matzinger, Lipopolysaccharide-activated dendritic cells: "Exhausted" or alert and waiting? *J. Immunol.* **188**, 5981–5989 (2012).
45. L. S. Carstensen, O. Lie-Andersen, A. Obers, M. D. Crowther, I. M. Svane, M. Hansen, Long-term exposure to inflammation induces differential cytokine patterns and apoptosis in dendritic cells. *Front. Immunol.* **10**, 2702 (2019).
46. A. Alloatti, F. Kotsias, A. M. Pauwels, J. M. Carpier, M. Jouve, E. Timmerman, L. Pace, P. Vargas, M. Maurin, U. Gehrmann, L. Joannas, O. I. Vivar, A. M. Lennon-Duménil, A. Savina, K. Gevaert, R. Beyaert, E. Hoffmann, S. Amigorena, Toll-like receptor 4 engagement on dendritic cells restrains phago-lysosome fusion and promotes cross-presentation of antigens. *Immunity* **43**, 1087–1100 (2015).
47. B. C. Gil-Torregrosa, A. M. Lennon-Duménil, B. Kessler, P. Guermonprez, H. L. Ploegh, D. Fruci, P. Van Endert, S. Amigorena, Control of cross-presentation during dendritic cell maturation. *Eur. J. Immunol.* **34**, 398–407 (2004).
48. S. K. Wculek, J. Amores-Iniesta, R. Conde-Garrosa, S. C. Khouili, I. Melero, D. Sancho, Effective cancer immunotherapy by natural mouse conventional type-1 dendritic cells bearing dead tumor antigen. *J. Immunother. Cancer* **7**, 100 (2019).
49. J. Waaler, L. Mygland, A. Tveita, M. F. Strand, N. T. Solberg, P. A. Olsen, A. Aizenshtadt, M. Fauskanger, K. Lund, S. A. Brinch, M. Lycke, E. Dybing, V. Nygaard, S. L. Bøe, K. M. Heintz, E. Hovig, C. Hammarström, A. Corthay, S. Krauss, Tankyrase inhibition sensitizes melanoma to PD-1 immune checkpoint blockade in syngeneic mouse models. *Commun. Biol.* **3**, 196 (2020).
50. S. Kwak, J.-Y. Lee, M. J. Kim, H. J. Lee, D.-K. Lee, J. Kang, W.-h. Kang, W.-C. Son, D. J. M. Cruz, Combination of PD-1 checkpoint blockade and botulinum toxin type A1 improves antitumor responses in mouse tumor models of melanoma and colon carcinoma. *Immunol. Invest.* **52**, 749–766 (2023).
51. R. Ouchida, S. Yamasaki, M. Hikida, K. Masuda, K. Kawamura, A. Wada, S. Mochizuki, M. Tagawa, A. Sakamoto, M. Hatano, T. Tokuhisa, H. Koseki, T. Saito, T. Kurosaki, J. Y. Wang, A lysosomal protein negatively regulates surface T cell antigen receptor expression by promoting CD3ζ-chain degradation. *Immunity* **29**, 33–43 (2008).
52. W. Li, S. Qiu, J. Chen, S. Jiang, W. Chen, J. Jiang, F. Wang, W. Si, Y. Shu, P. Wei, G. Fan, R. Tian, H. Wu, C. Xu, H. Wang, Chimeric antigen receptor designed to prevent ubiquitination and downregulation showed durable antitumor efficacy. *Immunity* **53**, 456–470.e6 (2020).
53. M. Tkach, J. Kowal, A. E. Zucchetti, L. Enserink, M. Jouve, D. Lankar, M. Saitakis, L. Martin-jaular, C. Théry, Qualitative differences in T-cell activation by dendritic cell-derived extracellular vesicle subtypes. *EMBO J.* **36**, 3012–3028 (2017).
54. C. Sedlik, J. Vigneron, L. Torrieri-dramard, F. Pitoiset, J. Denizeau, C. Chesneau, P. De Rochere, O. Lantz, C. Thery, B. Bellier, Different immunogenicity but similar antitumor efficacy of two DNA vaccines coding for an antigen secreted in different membrane vesicle-associated forms. *J. Extracell. Vesicles* **3**, 1–13 (2014).
55. T. L. Murphy, M. G. Cleveland, P. Kulesza, J. Magram, K. M. Murphy, Regulation of interleukin 12 p40 expression through an NF-κB half-site. *Mol. Cell. Biol.* **15**, 5258–5267 (1995).
56. D. J. Propper, F. R. Balkwill, Harnessing cytokines and chemokines for cancer therapy. *Nat. Rev. Clin. Oncol.* **19**, 237–253 (2022).
57. R. Genolet, S. Bobisse, J. Chiffelle, M. Arnaud, R. Petremand, L. Queiroz, A. Michel, P. Reichenbach, J. Cesbron, A. Auger, P. Baumgaertner, P. Guillaume, J. Schmidt, M. Irving, L. E. Kandalaft, D. E. Speiser, G. Coukos, A. Harari, TCR sequencing and cloning methods for repertoire analysis and isolation of tumor-reactive TCRs. *Cell Rep. Methods* **3**, 100459 (2023).
58. Y. Li, J. Wang, L. Wu, X. Li, X. Zhang, G. Zhang, S. Xu, S. Sun, S. Jiao, Diversity of dominant peripheral T cell receptor clone and soluble immune checkpoint proteins associated with clinical outcomes following immune checkpoint inhibitor treatment in advanced cancers. *Front. Immunol.* **12**, 649343 (2021).
59. M. Morotti, A. J. Grimm, H. C. Hope, M. Arnaud, M. Desbuisson, N. Rayroux, D. Barras, M. Masid, B. Murgues, B. S. Chap, M. Ongaro, I. A. Rota, C. Ronet, A. Minasyan, J. Chiffelle, S. B. Lacher, S. Bobisse, C. Murgues, E. Ghisoni, K. Ouchen, R. Bou Mjahed, F. Benedetti, N. Abdellaoui, R. Turrini, P. O. Gannon, K. Zaman, P. Mathevet, L. Lelievre, I. Crespo, M. Conrad, G. Verdeil, L. E. Kandalaft, J. Dagher, J. Corria-Osorio, M. A. Doucey, P. C. Ho, A. Harari, N. Vannini, J. P. Böttcher, D. Dangaj Laniti, G. Coukos, PGE2 inhibits TIL expansion by disrupting IL-2 signalling and mitochondrial function. *Nature* **629**, 426–434 (2024).
60. N. J. Neubert, L. Tillé, D. Barras, C. Soneson, P. Baumgaertner, D. Rimoldi, D. Gfeller, M. Delorenzi, S. A. F. Marraco, D. E. Speiser, Broad and conserved immune regulation by genetically heterogeneous melanoma cells. *Cancer Res.* **77**, 1623–1636 (2017).
61. S. Pierini, R. Gabbasov, M. C. Oliveira-Nunes, R. Qureshi, A. Worth, S. Huang, K. Nagar, C. Griffin, L. Lian, Y. Yashiro-Ohtani, K. Ross, C. Sloas, M. Ball, B. Schott, P. Sonawane, L. Cornell, D. Blumenthal, S. Chhum, N. Minutolo, K. Ciccaglione, L. Shaw, I. Zentner, H. Levitsky, O. Shestova, S. Gill, B. Varghese, D. Cushing, S. Ceeraz DeLong, S. Abramson, T. Condamine, M. Klichinsky, Chimeric antigen receptor macrophages (CAR-M) sensitize HER2+ solid tumors to PD1 blockade in pre-clinical models. *Nat. Commun.* **16**, 706 (2025).
62. M. Klichinsky, M. Ruella, O. Shestova, X. M. Lu, A. Best, M. Zeeman, M. Schmierer, K. Gabrusiewicz, N. R. Anderson, N. E. Petty, K. D. Cummins, F. Shen, X. Shan, K. Veliz, K. Blouch, Y. Yashiro-Ohtani, S. S. Kenderian, M. Y. Kim, R. S. O'Connor, S. R. Wallace, M. S. Kozlowski, D. M. Marchione, M. Shestov, B. A. Garcia, C. H. June, S. Gill, Human chimeric antigen receptor macrophages for cancer immunotherapy. *Nat. Biotechnol.* **38**, 947–953 (2020).
63. A. Lei, H. Yu, S. Lu, H. Lu, X. Ding, T. Tan, H. Zhang, M. Zhu, L. Tian, X. Wang, S. Su, D. Xue, S. Zhang, W. Zhao, Y. Chen, W. Xie, L. Zhang, Y. Zhu, J. Zhao, W. Jiang, G. Church, F. K. M. Chan, Z. Gao, J. Zhang, A second-generation M1-polarized CAR macrophage with antitumor efficacy. *Nat. Immunol.* **25**, 102–116 (2024).
64. M. Kang, S. H. Lee, M. Kwon, J. Byun, D. Kim, C. Kim, S. Koo, S. P. Kwon, S. Moon, M. Jung, J. Hong, S. Go, S. Y. Song, J.-H. Choi, T. Hyeon, Y.-K. Oh, H. H. Park, B.-S. Kim, Nanocomplex-mediated in vivo programming to chimeric antigen receptor-M1 macrophages for cancer therapy. *Adv. Mater.* **33**, e2103258 (2021).
65. K. A. Reiss, M. G. Angelos, E. C. Dees, Y. Yuan, N. T. Ueno, P. R. Pohlmann, M. L. Johnson, J. Chao, O. Shestova, J. S. Serody, M. Schmierer, M. Kremp, M. Ball, R. Qureshi, B. H. Schott, P. Sonawane, S. C. DeLong, M. Christiano, R. F. Swaby, S. Abramson, K. Locke, D. Barton, E. Kennedy, S. Gill, D. Cushing, M. Klichinsky, T. Condamine, Y. Abdou, CAR-macrophage therapy for HER2-overexpressing advanced solid tumors: A phase 1 trial. *Nat. Med.* **31**, 1171–1182 (2025).
66. A. Alloatti, F. Kotsias, J. G. Magalhaes, S. Amigorena, Dendritic cell maturation and cross-presentation: Timing matters! *Immunol. Rev.* **272**, 97–108 (2016).
67. A. Langenkamp, M. Messi, A. Lanzavecchia, F. Sallusto, Kinetics of dendritic cell activation: Impact on priming of T_H1, T_H2 and nonpolarized T cells. *Nat. Immunol.* **1**, 311–316 (2000).
68. C. R. e Sousa, Dendritic cells in a mature age. *Nat. Rev. Immunol.* **6**, 476–483 (2006).

69. K. L. Hilligan, F. Ronchese, Antigen presentation by dendritic cells and their instruction of CD4+ T helper cell responses. *Cell. Mol. Immunol.* **17**, 587–599 (2020).
70. F. Junker, J. Gordon, O. Qureshi, Fc gamma receptors and their role in antigen uptake, presentation, and T cell activation. *Front. Immunol.* **11**, 1393 (2020).
71. P. Boross, N. van Montfoort, D. A. C. Stapels, C. E. van der Poel, C. Bertens, J. Meeldijk, J. H. M. Jansen, J. S. Verbeek, F. Ossendorp, R. Wubbolts, J. H. W. Leusen, FcRγ-chain ITAM signaling is critically required for cross-presentation of soluble antibody–antigen complexes by dendritic cells. *J. Immunol.* **193**, 5506–5514 (2014).
72. S. Kleffel, C. Posch, S. R. Barthel, H. Mueller, C. Schlapbach, E. Guenova, C. P. Elco, N. Lee, V. R. Juneja, Q. Zhan, C. G. Lian, R. Thomi, W. Hoetzenecker, A. Cozzio, R. Dummer, M. C. Mihm, K. T. Flaherty, M. H. Frank, G. F. Murphy, A. H. Sharpe, T. S. Kupper, T. Schatton, Melanoma cell-intrinsic PD-1 receptor functions promote tumor growth. *Cell* **162**, 1242–1256 (2015).
73. P. Brossart, The role of antigen spreading in the efficacy of immunotherapies. *Clin. Cancer Res.* **26**, 4442–4447 (2020).
74. P. Reichenbach, G. M. P. Giordano Attianese, K. Ouchen, E. Cribioli, M. Triboulet, S. Ash, M. Saillard, R. Vuillefroy de Silly, G. Coukos, M. Irving, A lentiviral vector for the production of T cells with an inducible transgene and a constitutively expressed tumour-targeting receptor. *Nat. Biomed. Eng.* **7**, 1063–1080 (2023).
75. R. Uchibori, T. Teruya, H. Ido, K. Ohmine, Y. Sehara, M. Urabe, H. Mizukami, J. Mineno, K. Ozawa, Functional analysis of an inducible promoter driven by activation signals from a chimeric antigen receptor. *Mol. Ther. Oncolytics* **12**, 16–25 (2019).
76. K. D. Moynihan, C. F. Opel, G. L. Szeto, A. Tzeng, E. F. Zhu, J. M. Engreitz, R. T. Williams, K. Rakhra, M. H. Zhang, A. M. Rothschilds, S. Kumari, R. L. Kelly, B. H. Kwan, W. Abraham, K. Hu, N. K. Mehta, M. J. Kauke, H. Suh, J. R. Cochran, D. A. Lauffenburger, K. D. Wittrup, D. J. Irvine, Eradication of large established tumors in mice by combination immunotherapy that engages innate and adaptive immune responses. *Nat. Med.* **22**, 1402–1410 (2016).
77. I. Keklikoglou, C. Cianciaruso, E. Güç, M. L. Squadrito, L. M. Spring, S. Tazzyman, L. Lambein, A. Poissonnier, G. B. Ferraro, C. Baer, A. Cassará, A. Guichard, M. L. Iruela-Arispe, C. E. Lewis, L. M. Coussens, A. Bardia, R. K. Jain, J. W. Pollard, M. De Palma, Chemotherapy elicits pro-metastatic extracellular vesicles in breast cancer models. *Nat. Cell Biol.* **21**, 190–202 (2019).
78. M. De Palma, L. Naldini, Transduction of a gene expression cassette using advanced generation lentiviral vectors. *Methods Enzymol.* **346**, 514–529 (2002).
79. S. Bobadilla, N. Sunseri, N. R. Landau, Efficient transduction of myeloid cells by an HIV-1-derived lentiviral vector that packages the Vpx accessory protein. *Gene Ther.* **20**, 514–520 (2013).
80. K. A. Hogquist, S. C. Jameson, W. R. Heath, J. L. Howard, M. J. Bevan, F. R. Carbone, T cell receptor antagonist peptides induce positive selection. *Cell* **76**, 17–27 (1994).
81. J. Holst, A. L. Szymczak-Workman, K. M. Vignali, A. R. Burton, C. J. Workman, D. A. A. Vignali, Generation of T-cell receptor retrogenic mice. *Nat. Protoc.* **1**, 406–417 (2006).

Acknowledgments: We thank C. Rmili-Wyser for managing mouse colonies and B. Mangeat (Gene Expression Core Facility, EPFL) for performing bulk RNA-seq. We also thank B. Correia, L. Scheller, D. Constam, L. Tang (all EPFL), L. Kandalaft, and L. Beziaud (University of Lausanne) for advice on some experiments and for providing materials. Schematics were created in BioRender. **Funding:** This study was supported by grants from the Swiss Cancer Research Foundation/Swiss Cancer League (KLS-4505-08-2018 to M.D.P.), European Research Council (ERC CoG EVOLVE-725051 to M.D.P.), Swiss National Science Foundation (SNSF CRSII5_189967 to M.D.P.), and ISREC Foundation (TANDEM to M.D.P. and N.M.). K.J. was supported by the Austrian Science Fund (FWF; DK-MCD 10.55776/W1226). **Author contributions:** Y.M. designed and executed most of the experiments, analyzed and interpreted the results, and wrote the manuscript; V.G., O.E., G.C.R., J.J.v.d.S., A. Ghasem, K.J., B.T., A. Guichard, A.M.-U., and A.K. contributed to experiments involving cell cultures and mouse tumor models; R.G. performed TCR-seq; R.M. and N.F. analyzed and interpreted RNA-seq and TCR-seq data; T.V.P., D.E.S., S.J.R., and N.M. provided critical reagents and participated in experimental design and data interpretation; M.D.P. designed experiments, interpreted the results, coordinated the study, and wrote the manuscript. All authors reviewed and edited the manuscript. **Competing interests:** M.D.P. has received sponsored research grants from EVIR Therapeutics, Hoffmann La-Roche, and Deciphera Pharmaceuticals and has served on the scientific advisory boards of EVIR Therapeutics, Montis Biosciences, Macomics, Laverock Therapeutics, Deciphera Pharmaceuticals, Light Chain Bioscience/Novimmune, and Genenta. M.D.P., Y.M., A. Ghasem, and A.M.-U. are inventors on patents WO/2017/134100 and WO/2023/232777 and application no. 24211693.7 filed by EPFL, which cover methods for DC engineering. R.G. is an inventor on patent WO2018144410A filed by UNIL and Ludwig Institute for Cancer Research, which covers methods for TCR sequencing. The other authors declare that they have no competing interests. **Data and materials availability:** All data associated with this study are present in the paper or the Supplementary Materials. Raw numerical data (with $n < 20$) associated with this study are presented in data file S1. RNA-seq and TCR-seq data have been deposited in Gene Expression Omnibus (GEO) with GEO accession GSE266100. All reagents and constructs used in this study are either commercially available or can be made available to academic researchers from the corresponding author upon reasonable request. No custom code was generated for this study.

Submitted 12 May 2024
Resubmitted 6 April 2025
Accepted 24 November 2025
Published 17 December 2025
10.1126/scitranslmed.adq4060